Technical report; TR-234

KNMI

Evaluation of a plant physiological canopy conductance model in the ECMWF land surface scheme

J. van de Kassteele

De Bilt, 2001

Koninklijk Nederlands Meteorologisch Instituut

Technical Report = Technisch Rapport; TR-234

De Bilt, 2001

PO Box 201, 3730 AE De Bilt
The Netherlands
Wilhelminalaan 10
http://www.knmi.nl
Telephone +31 30 22 06 911
Telefax +31 30 22 10 407

Author: J. van de Kassteele

UDC: 551.551.8
551.509.3
551.584.4

ISSN: 0169-1708

ISBN: 90-369-2195-3

Evaluation of a plant physiological canopy conductance model in the ECMWF land surface scheme

Author:
J. van de Kassteele
(Meteorology and Air Quality Group, Wageningen University)

Supervisor:
B.J.J.M. van den Hurk
(KNMI)

Abstract

A new representation of the canopy conductance in large scale atmospheric models, based on plant physiological theory, is evaluated. Calibration parameters for this canopy conductance model are considered to be more universal than the coefficients in the empirical relations used in many current large scale models. The new conductance model is compared with an empirical so-called Jarvis-Stewart approach in the ECMWF land surface scheme. A priori settings of model parameters were used for all vegetation types except for needle-leaf forests, for which model parameters have been tuned using field observations.
The behaviour under different environmental conditions is examined. It is concluded that in the new model synergetic relations exist between the environmental variables, which are not present in the empirical approach.
The new model is implemented in the ECMWF land surface scheme. It is tested in offline mode with data from five surface field campaigns with different surface characteristics and vegetation types. In general the mean error and scatter have become smaller. The best results were obtained for low vegetation surfaces.
Furthermore the new plant physiological approach is tested in the 3D Regional Atmospheric Climate Model RACMO where it is compared with the empirical Jarvis-Stewart approach. One important aspect is that the evaporation has increased. Three subdomains were analysed separately, representing areas dominated by low vegetation, high vegetation, and needle-leaf forests. Comparing the modelled 2m relative humidity and temperature with observations for these areas it is concluded that the bias has become larger, but the root mean square error has become smaller in the new approach. Again the best results were obtained for low vegetation surfaces.

Contents

1. Introduction

In modelling the surface energy budget it is important to know the turbulent fluxes of sensible and latent heat. Mostly these fluxes are parameterised in terms of a temperature or humidity difference between a reference level in the atmosphere and the surface. The coupling between the fluxes and the temperature or humidity differences can by represented by a resistance. For the sensible heat flux this resistance is called the aerodynamic resistance. For the latent heat flux over a layer of vegetation, which is a large percentage of surfaces in the world, a second resistance is needed, the canopy resistance. It determines the partitioning of available energy over the sensible and latent heat flux density.

The canopy resistance, or its reciprocal value, the canopy conductance, depends on different environmental factors as light intensity, atmospheric vapour pressure deficit, leaf temperature and available soil moisture. In most atmospheric models, the canopy conductance is calculated as a maximum conductance reduced by so called stress functions, which are related to variables at an atmospheric reference level. This approach is usually referred to as the Jarvis-Stewart (JS) approach (Jarvis, 1976; Stewart, 1988). The stress functions in this approach are empirically obtained and based on statistics. In climate models the question can rise, whether the stress functions still hold when carbon dioxide concentrations increase.

Another approach is the so-called A-gs approach. Here the stomatal conductance g_s is related to the plant assimilation rate A and the external CO_2 concentration (Jacobs, 1994; Ronda et al., 2001). The stomatal resistance is scaled up from leaf to canopy. The A-gs model is a plant physiological model and the model parameters are generally based on the distinction in C3 and C4 plants. The stress functions are obtained under different (laboratory) climates and are considered to be more robust than the statistical empirical approach. The A-gs approach should be able to compute the canopy conductance a priori in stead of using local optimisation (Ronda et al., 2001).

The objective of this study is to evaluate whether the implementation of the A-gs model leads to improved estimates of the surface energy balance flux densities and the hydrological quantities, such as cumulative evaporation, run-off and soil moisture content, for the entire European continent.

The A-gs model described by Ronda et al. (2001) is implemented in the ECMWF surface scheme (Van den Hurk et al., 2000) in the Regional Atmospheric Climate Model RACMO. In chapter 2 a brief description of the ECMWF surface scheme will be given and the two approaches to compute the canopy conductance will be discussed. Then in chapter 3, the A-gs model is validated offline for some different surfaces ranging from short grass to needle-leaf forests. In chapter 4, a 3D evaluation performed to see the effect of the A-gs approach in a 3D atmospheric model. Both chapters 3 and 4 will be closed with a summary and conclusions. Finally, in chapter 5 recommendations for further research will be given.

2. Model descriptions

2.1 Brief description of the ECMWF surface scheme

Each grid box of the ECMWF land surface scheme is divided in different surface fractions or tiles. The surface energy balance is separately solved for each tile. This results in different turbulent fluxes and skin temperatures for each tile. The tiles are connected to the atmosphere (lowest model level) and soil. Eight tiles are distinguished: (Van den Hurk et al., 2000)

1. Water (ocean and lake)
2. Sea ice
3. Interception layer
4. Dry low vegetation
5. Snow on bare ground and low vegetation
6. Dry high vegetation
7. Snow under high vegetation
8. Bare ground

Each tile is characterised by a set of coefficients, namely the fractional coverage, the skin conductivity (to calculate the soil heat flux) and the fraction of net shortwave radiation that is absorbed in the skin layer.
Low and high vegetation are treated separately. For each grid box one low vegetation type and one high vegetation type is selected. Each vegetation type is characterised by a vegetation coverage c_{veg}, a leaf area index *LAI* and the root distribution over the soil layers (Van den Hurk et al., 2000). In the control model (original scheme using the JS-approach) also a minimum stomatal resistance $r_{s,min}$ and a sensitivity coefficient g_D for the dependence of the canopy resistance on vapour pressure deficit are given. In the A-gs model a label indicating the plant type replaces these two parameters: C3, C4 or needle-leaf plant type. In table 2.1 a summary of the vegetation types and their parameter values is given. The vegetation types are based on the classification of the BATS surface scheme (Dickinson et al.,1993), as given in the USGS (1999) dataset. For further details see Van den Hurk et al. (2000).
For the European continent all vegetation types may be considered as C3 plants. Some crops (such as maize) can be given a C4 label, but for practical reason this is not done. The needle-leaf trees are given a needle-leaf label (see section 2.3).

2.2 The empirical and A-gs approach in the ECMWF surface scheme

The empirical JS-approach used in the ECMWF surface scheme is described in Van den Hurk et al. (2000). The canopy conductance is a function of the maximum stomatal conductance $g_{s,max}$ (the reciprocal value of $r_{s,min}$ in table 2.1), the downward shortwave radiation $K^{\downarrow}$, leaf area index *LAI*, average soil moisture content θ and atmospheric vapour pressure deficit D_a:

$$g_c = g_{s,\max} LAI f_1(K^{\downarrow}) f_2(\theta) f_3(D_a) \tag{2.1}$$

The stress functions are specified according to Van den Hurk et al. (2000) as follows:

$$f_1(K^{\downarrow}) = \min\left[1, \frac{bK^{\downarrow} + c}{a(1 + bK^{\downarrow})}\right] \tag{2.2}$$

Table 2.1. Vegetation types and parameter values (Van den Hurk et al., 2000). The root distribution parameters are not shown. In the A-gs model $r_{s,min}$ and g_D are replaced by the plant type label.

index	vegetation type	L/H veg	c_{veg} [-]	LAI [$m^2\ m^{-2}$]	$r_{s,min}$ [$s\ m^{-1}$]	g_D [mb^{-1}]	plant type
1	crops, mixed farming	L	0.90	3	180	0	C3
2	short grass	L	0.85	2	110	0	C3
3	evergreen needle-leaf trees	H	0.90	5	500	0.03	needle
4	deciduous needle-leaf trees	H	0.90	5	500	0.03	needle
5	deciduous broadleaf trees	H	0.90	5	175	0.03	C3
6	evergreen broadleaf trees	H	0.99	6	240	0.03	C3
7	tall grass	L	0.70	2	100	0	C3
8	desert	L	0.00	0.5	250	0	C3
9	tundra	L	0.50	1	80	0	C3
10	irrigated crops	L	0.90	3	180	0	C3
11	semidesert	L	0.10	0.5	150	0	C3
12	ice caps and glaciers	-	-	-	-	-	-
13	bogs and marshes	L	0.60	4	240	0	C3
14	inland water	-	-	-	-	-	-
15	ocean	-	-	-	-	-	-
16	evergreen shrubs	L	0.50	3	225	0	C3
17	deciduous shrubs	L	0.50	1.5	225	0	C3
18	mixed forest/woodland	H	0.90	5	250	0.03	C3
19	interrupted forest	H	0.90	2.5	175	0.03	C3
20	water and land mixtures	L	0.60	4	150	0	C3

where a, b and c are empirical constants. Function f_2 is a linear function of the root-weighted averaged soil moisture content:

$$f_2(\theta) = \begin{cases} 0 & \theta < \theta_{pwp} \\ \dfrac{\theta - \theta_{pwp}}{\theta_{cap} - \theta_{pwp}} & \theta_{pwp} \le \theta < \theta_{cap} \\ 1 & \theta \ge \theta_{cap} \end{cases} \tag{2.3}$$

where θ_{pwp} is the soil moisture content at permanent wilting point and θ_{cap} the soil moisture content at field capacity. The following relation gives the dependence on atmospheric vapour deficit. The parameter g_D exceeds zero for high vegetation only (see table 2.1).

$$f_3(D_a) = e^{-g_D D_a} \tag{2.4}$$

In the A-gs approach a plant physiological model is used where the stomatal conductance (and therefore the water vapour flow) is related with the CO_2 assimilation rate. See figure 2.1. The canopy conductance is computed as a function of the photosynthetic active radiation PAR, the skin temperature T_{sk}, the external CO_2 concentration C_a, leaf area index LAI, vapour pressure deficit at plant level D_s and average soil moisture content θ:

$$g_c = f(PAR, T_{sk}, C_a, LAI, D_s) f_2(\theta) \tag{2.5}$$

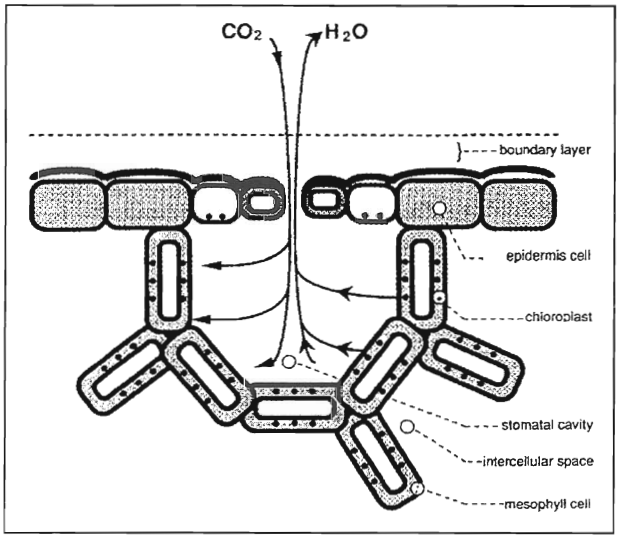

Figure 2.1. Cross-section of a leaf through a stoma (Lövenstein et al., 1995).

The function f is the plant physiological model (Ronda et al., 2001) which is independent of the second soil moisture stress function. To calculate the canopy conductance g_c, first the stomatal conductance g_s must be computed. It is given by:

$$g_s = g_{\min,c} + \frac{a_1 A_g}{(C_a - \Gamma)(1 + \frac{D_s}{D_*})} \tag{2.6}$$

where $g_{min,c}$ is the cuticular conductance, the conductance when the stomata are fully closed, A_g the gross assimilation rate ($= f(PAR, T_{sk}, C_i)$, C_i being the CO_2 concentration inside the stomatal cavities), Γ the CO_2 compensation point, $a_1 = 1 / (1 - f_0)$ and $D_* = D_0 / (a_1 - 1)$ (see below). The internal/external CO_2 ratio is given by a linear function of the atmospheric vapour pressure deficit at plant level (Zhang and Nobel, 1996):

$$\frac{C_i - \Gamma}{C_a - \Gamma} = f_0 - a_d D_s \tag{2.7}$$

f_0 is the maximum C_i/C_a ratio for stomata without humidity stress. a_d is an empirical parameter describing the dependency of the C_i/C_a ratio on the atmospheric vapour pressure deficit. Finally, the maximum vapour pressure deficit where the stomata fully close and the vegetation does not react to an increasing drought anymore, D_0, is given by

$$D_0 = \frac{f_0 - f_{\min}}{a_d} \tag{2.8}$$

Here f_{min} is the minimum C_i/C_a ratio.
Scaling the stomatal conductance up to the canopy level, the resulting expression becomes:

$$g_c = g_{\min,c} LAI + \frac{a_1 (A_m + R_d)}{(C_a - \Gamma)\left(1 + \frac{D_s}{D_*}\right)} \left[LAI - \frac{1}{K_x} \left(E_1 \left(\frac{\alpha K_x PAR_t}{A_m + R_d} e^{-K_x LAI} \right) - E_1 \left(\frac{\alpha K_x PAR_t}{A_m + R_d} \right) \right) \right] \quad (2.9)$$

A_m and R_d are the primary production and the dark respiration respectively, α is the light use efficiency, K_x is the vegetation extinction coefficient, PAR_t is the photosynthetic active radiation at the top of the canopy and $E_1(x)$ is the exponential integral with argument x.
A quadratic soil moisture stress function, as described by Ronda et al. (2001), is applied for the A-gs approach, which should give a better physical representation under dry conditions:

$$f_2(\theta) = 2\beta(\theta) - [\beta(\theta)]^2 \quad (2.10)$$

where

$$\beta(\theta) = \begin{cases} 0 & \theta < \theta_{pwp} \\ \dfrac{\theta - \theta_{pwp}}{\theta_{cap} - \theta_{pwp}} & \theta_{pwp} \le \theta < \theta_{cap} \\ 1 & \theta \ge \theta_{cap} \end{cases} \quad (2.11)$$

With this set of equations a plant physiological model is given to compute the canopy conductance for low vegetation (Ronda et al., 2001). This model has not been validated for high vegetation. It is assumed the model is suitable for broad leaf trees. For needle-leaf trees some adjustments are applied. These adjustments will be discussed in the next section.

2.3 The A-gs model for needle-leaf trees

Former runs of the RACMO with the A-gs model showed an excessive evaporation for needle-leaf forests, especially during summer. The modelled latent heat flux frequently was a factor two to three higher than the observations.
This excessive evaporation can be attributed to a physical process that has not been implemented in the current A-gs model. Needles are covered with a wax coating which causes an extra resistance to the water vapour and CO_2 flow (see figure 2.1). Several options to include this effect in the A-gs model are available, but still no solution is satisfactorily.
The most trivial solution is to apply an extra resistance to the equations of the A-gs given by Ronda et al. (2001). Unfortunately, the extra resistance resulted in significant difficulties in solving the equations (2.5) – (2.9). Because this solution certainly is the most elegant one, it may be a point for further research.
The pragmatic solution was chosen to solve the problem: tuning the model parameters. Some parameters are unchanged compared to the C3-values, such as the initial light use efficiency α_0, the CO_2 compensation point Γ, the mesophyll conductance g_m and the maximum primary production $A_{m,max}$. Others are assumed to change by introducing an extra resistance. The parameters tuned in this study are the maximum C_i/C_a ratio f_0, the slope giving the dependence of the C_i/C_a ratio on the water vapour pressure deficit a_d, and the cuticular conductance $g_{min,c}$. The three model parameters were optimised using three years of BOREAS data (see section 3.1.4). The sum of the squared modelled latent heat flux minus the observed

Table 2.2. Parameter values of the biochemical model.

plant type	Parameter	X (T_{sk} = 298 K)	Q_{10}	T_1 [K]	T_2 [K]
C3	α_0 [mg J^{-1}]	0.017			
	Γ [mg m^{-3}]	68.5ρ_a	1.5		
	g_m [mm s^{-1}]	7.0	2.0	278	301
	$A_{m,max}$ [mg m^{-2} s^{-1}]	2.2	2.0	281	311
	f_0 [-]	0.89			
	a_d [kPa^{-1}]	0.07			
	$g_{min,c}$ [mm s^{-1}]	0.25			
C4	α_0 [mg J^{-1}]	0.015			
	Γ [mg m^{-3}]	4.3ρ_a	1.5		
	g_m [mm s^{-1}]	17.5	2.0	286	309
	$A_{m,max}$ [mg m^{-2} s^{-1}]	2.2	2.0	286	311
	f_0 [-]	0.85			
	a_d [kPa^{-1}]	0.015			
	$g_{min,c}$ [mm s^{-1}]	0.25			
needle-leaf	α_0 [mg J^{-1}]	0.017			
	Γ [mg m^{-3}]	68.5ρ_a	1.5		
	g_m [mm s^{-1}]	7.0	2.0	278	301
	$A_{m,max}$ [mg m^{-2} s^{-1}]	2.2	2.0	281	311
	f_0 [-]	0.4			
	a_d [kPa^{-1}]	0.12			
	$g_{min,c}$ [mm s^{-1}]	0			

latent heat flux around local noon was used as error indicator.
The optimal cuticular conductance $g_{min,c}$ was found to be equal to 0, the f_0 value 0.4 and the slope a_d 0.12 kPa^{-1}. The final model parameters for C3, C4 and needle-leaf plants are given in table 2.2 (after Ronda et al., 2001). For a complete explanation of the model parameters, see section 2.4.
In figure 2.2 the relation between the vapour pressure deficit and the C_i/C_a ratio is shown for C3 needle-leaf trees without the wax coating and needle-leaf trees with wax coating, using the optimised values of table 2.2. Figure 2.3 shows the canopy conductance for the two plant types, including the canopy conductance according to the JS-approach. Typical values for the LAI and $r_{s,min}$ are taken from table 2.1. As can be seen, the canopy conductance is much higher for the unadjusted A-gs model. Due to the optimisation, the canopy conductance is similar to the JS-calibration when $D_s = 0$.

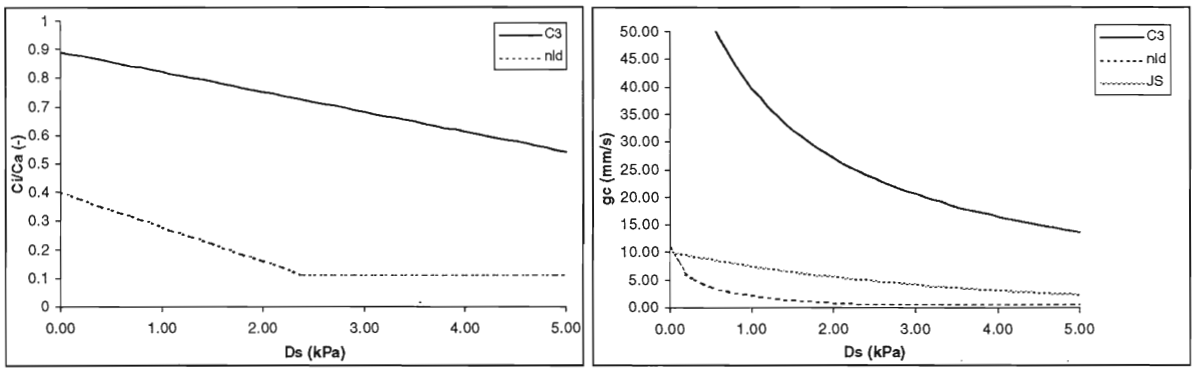

Figure 2.2 and 2.3. The C_i/C_a ratio (left) and the canopy conductance (right) for the unadjusted A-gs model (C3), the adjusted A-gs model for needle-leaf vegetation (nld) and the empirical JS-approach.

2.4 Sensitivity of the A-gs model to changing model parameters

In the previous section a summary was given of the seven model parameters for the different plant types. In this section a sensitivity study on the canopy conductance to changing model parameters under different environmental conditions is done to investigate which parameters are important in the A-gs model.
In table 2.3 a summary is given. The model parameter values are 10% increased and the relative change (%) in the canopy conductance is given for four conditions, ranging from low stress conditions (high light intensity and no water vapour stress) to high stress conditions (low light intensity and dry conditions). The following reference values are taken: T_{sk} = 20 °C, LAI = 2 m^2/m^2, high PAR = 400 W/m^2, low PAR = 50 W/m^2 and high D_s = 5 kPa.

Table 2.3. Relative change in the canopy conductance (C3 plant) for a 10% increased model parameter value under different environmental conditions.

Parameter	PAR = 400 D_s = 0	PAR = 400 D_s = 5	PAR = 50 D_s = 0	PAR = 50 D_s = 5
α_0	4.0	2.9	8.3	6.2
Γ	-0.4	-0.2	-1.4	-0.7
g_m	2.2	4.4	0.3	1.5
$A_{m,max}$	2.9	2.0	0.5	0.4
f_0	428.6	25.9	397.2	16.4
a_d	0.0	-9.2	0.0	-5.5
$g_{min,c}$	0.2	0.0	0.7	2.2
K_x	0.8	0.4	3.3	2.6

The A-gs model is relatively sensitive to initial light use efficiency α_0. This parameter determines the dependence of the assimilation rate at low light intensities, so a relative high change in the canopy conductance can be seen for low PAR values. Increasing vapour pressure deficit reduces the sensibility to α_0.
As can be seen from table 2.3, the CO_2 compensation point Γ has only a small influence on the canopy conductance. This parameter determines the point where the respiration rate is in equilibrium with the assimilation rate. Therefore the largest effect is seen at low light intensities. Γ increases with temperature.
The mesophyll conductance g_m is the conductance for CO_2 between the stomatal cavity and the mesophyll cells where the photosynthesis takes place. At high light intensities, the photosynthesis rate is higher, so the influence of the mesophyll conductance is larger.
The maximum primary production $A_{m,max}$ is the assimilation rate under optimal light, temperature and vapour pressure deficit conditions. Therefore the relative effect of $A_{m,max}$ is largest under optimal conditions: high PAR and low D_s. Both g_m and $A_{m,max}$ are a function of the temperature, showing an optimum around 25°C (298 K).
The A-gs model is most sensitive to the parameter f_0, the maximum C_i/C_a ratio for stomata without humidity stress. The higher this value, the more CO_2 is available for assimilation. Because the stomata are fully open at saturation (D_s = 0), the largest effect is seen there. The effect is larger under high light intensities.
a_d is the parameter describing the dependency of the C_i/C_a ratio on the atmospheric vapour pressure deficit. No effect is seen at D_s = 0 (see equation (2.7)). Only at higher values of D_s, a_d affects the canopy conductance. In contrast to f_0, a high value for a_d reduces the available CO_2 for assimilation and thus reduces the canopy conductance.

The cuticular conductance $g_{min,c}$ is the conductance when the stomata are fully closed. This parameter, which in fact is an extra term in equation (2.9), has the largest influence at low assimilation rates, because then this term is relatively large compared to the second term of equation (2.9).
Finally, the vegetation extinction coefficient K_x determines the vertical distribution of *PAR* over the canopy. A higher value of K_x will mean that more *PAR* is absorbed, so higher assimilation rates can be achieved. This effect is only present at low light intensities.

2.5 Comparison of the dependence of the A-gs and JS-approach on environmental conditions

In the A-gs approach, the canopy conductance is computed from the environmental variables, taken into account the synergetic effects. For that reason, it is better not to speak about stress functions as in the JS-approach. However, to compare the A-gs model with the empirical statistical JS-approach, the normalised canopy conductance can be computed for different conditions, so eventually they can be compared. The normalised canopy conductance is the canopy conductance relative to the maximum canopy conductance (i.e. the conductance without stress).
For an indication, in figure 2.4 the dependency of the normalised canopy conductance is plotted against one environmental variable. The other variables are kept constant and do not induce any stress, so only the effect of one variable is shown. The vegetation is a typical grassland and parameters are similar to table 2.1. Unless mentioned otherwise, T_{sk} = 20 °C, *PAR* = 400 W/m^2, D_s = 0 kPa, *LAI* = 2 m^2/m^2 and $r_{s,min}$ = 110 s/m. Both a C3 plant type and the JS-approach are shown.
In table 2.4 the results of a qualitative study, where the dependency of the normalised canopy conductance on one environmental variable to an increase of the others, is shown. With a larger dependency on an environmental variable it is meant that this variable is becoming a limiting factor in the biochemical processes. For example, the PAR is becoming a limiting factor when the LAI increases.

Table 2.4. Dependency of the normalised canopy conductance on one environmental variable to an increase of the other variables.

Dependency on	*LAI* ↑	*PAR* ↑	D_s ↑	T_{sk} → opt
LAI	-	smaller	larger	smaller
PAR	larger	-	smaller	larger
D_s	smaller	smaller	-	larger
T_{sk}	smaller	larger	smaller	-

In general, an increase of *PAR* leads to an increase in the (normalised) canopy conductance. An increased *LAI* leads to a larger dependency on the *PAR*. A higher vapour pressure deficit D_s leads to a smaller dependency on the *PAR*. When the skin temperature T_{sk} goes to optimum, the dependency on the *PAR* increases.
The (normalised) canopy conductance decreases with an increased vapour pressure deficit until a certain minimum where the stomata close. A higher *LAI* leads to a smaller dependency on D_s, especially at low *PAR*. Increased *PAR* leads to smaller dependency on D_s. When T_{sk} goes to optimum, the dependency on D_s increases.
The dependency of the (normalised) canopy conductance on the skin temperature shows an optimum curve. A higher *LAI* leads to a smaller dependency on T_{sk}. An increase of the *PAR* leads to a larger dependency on T_{sk}. A higher vapour pressure deficit leads to a smaller

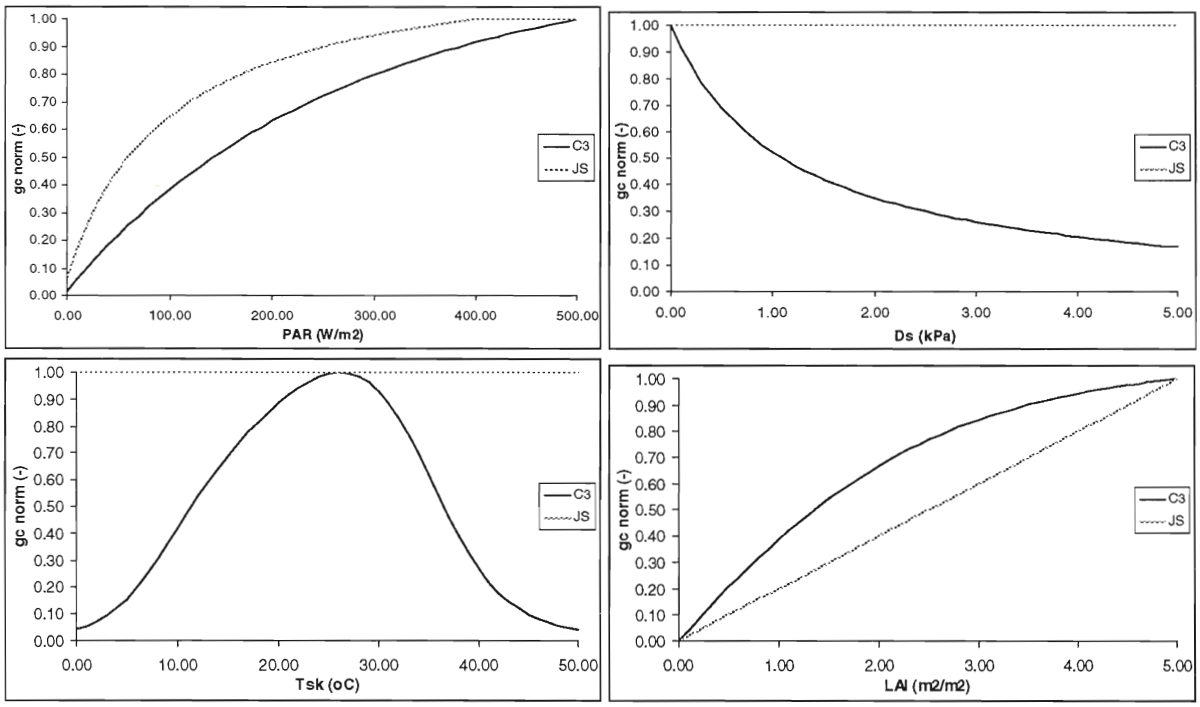

Figure 2.4. Normalised canopy conductance as a function of the PAR, D_s, T_{sk} and LAI for the A-gs model (C3 plant type) and the empirical JS-approach.

dependency on T_{sk}.

The (normalised) canopy conductance increases with higher *LAI*. An increase of *PAR* shows an optimum curve, with smaller dependency for optimum *PAR*. A higher vapour pressure deficit leads to a larger dependency on the *LAI*. When the skin temperature goes to optimum, the dependency on the *LAI* decreases.

For all environmental conditions the JS-approach shows no change of sensitivity to one variable when another variable changes. An important conclusion can be drawn from this study: in the A-gs model light, temperature, leaf area index and humidity stress are coupled. There is no synergetic relation between the environmental variables in the JS-approach.

3. Offline validation of the A-gs model

3.1 Data descripiton

Five sites were chosen for the offline validation of the A-gs model. First the Cabauw site was chosen for its typical low vegetation C3 type grassland. The FIFE site was chosen to validate the model's performance for C4 type grassland. The ARME site was chosen for its high vegetation broadleaf C3 plant type surface and finally the BOREAS and the Garderen site for their high-vegetation needle-leaf C3 plant type surfaces. In the next sections descriptions will be given of the sites. The descriptions are adapted from Van den Hurk et al. (2000). In table 3.1 a summary is given of the surface characteristics.

3.1.1 Cabauw

Beljaars and Bosveld (1997) prepared the Cabauw-1987 dataset (51.97°N, 4.93°E) for the PILPS intercomparison study reported by Chen et al. (1997). Observations are taken at a grassland site near the 200 m meteorological observation tower. The surface sensible heat flux is obtained from the profile method, and the latent heat flux calculated as a residual of the surface energy balance. Beljaars and Bosveld (1997) have performed extensive data quality checking and gap interpolation.
Data from this site are collected in a nearly continuous monitoring program. They have for instance been used for studies on evaporation of wet grassland (Beljaars and Viterbo, 1994), roughness length ratio (Beljaars and Holtslag, 1991) and interaction between land surface and planetary boundary layer (Ek and Holtslag, 1999).

3.1.2 FIFE

The dataset from the First ISLSCP Field Experiment (FIFE) was prepared by Betts and Ball (1998). Near surface meteorological quantities and radiative forcings were aggregated from carefully cleaned measurements from 10 automatic weather stations. Large gaps occurred in the measurement record of downward longwave and shortwave radiation, in particular in the winter and spring of 1987-1988. These data were replaced by closest grid point calculations from the ECMWF ERA15 cycle. ERA15 shortwave radiation data were reduced to 92% of their original value, in order to get the closest correspondence with local FIFE measurements. ERA15 data were linearly interpolated in time, matching the original time resolution. Wind speed was observed at 5.4 m height. A neutral logarithmic profile was assumed to extrapolate observed wind speeds to 2 m height.
Gaps in the forcings were interpolated by either a linear interpolation (wind, pressure) or by a trend in the diurnal cycles (temperature). Specific humidity was calculated from an interpolated relative humidity, to avoid super-saturation.
A site averaged surface flux dataset was constructed from available measurements during the summer months in 1987 and 1988. Eddy-correlation measurements were conducted during four intensive field campaigns in 1987 (including up to 22 surface flux stations), and outside these campaigns flux data are obtained by Bowen ratio devices. In 1989 flux measurements are available only during a short intensive observation period.

3.1.3 ARME

Shuttleworth et al. (1984) describe observations of forcings and energy fluxes over a representative terra firma forest site in the Brazilian part of the Amazonian tropical forest area. More than two years of hourly observations of standard meteorological and radiation forcings were collected during this ARME (Amazonian Regional Meteorological Experiment) campaign in the Ducke Reserve near Manaus (2.95°S, 59.95°W). Observations were taken at approximately 10 m above the canopy. The roughness length of the site was estimated to be 1.7 m, while z/z_{0m} was assumed to be approximately 10.4 (z being the measurement height above the displacement level), resulting in an estimated value for z of ± 18 m.
Fluxes of sensible heat and latent heat were measured using 1-dimensional eddy-correlation during selected time intervals. Shuttleworth (1988) analysed the data using a calibrated model describing the forest evaporation. An estimate of the monthly total evaporation and interception loss was provided.

3.1.4 BOREAS

Forcing data for the years 1994-1996 were taken from the so-called BOREAS MESONET observation network (Shewchuk, 1998) for two BOREAS Northern Study Area (NSA) sites (#8, near Thompson, Manitoba, at 55.80°N, 97.87°W, 221 m above sea level, mixed spruce and poplar with a thick moss understory and #9, 54.67°N, 101.69°W, 305 m above sea level, old jack pine in sandy soil with thin lichen surface). Observation height at both sites was 18 m, 5 m above the canopy top. Data from these sites were quality checked, averaged and missing data were interpolated, if necessary. If possible, downward longwave radiation was derived from a radiation balance equation using observed net radiation and skin temperature. Interpolation of long gaps of shortwave radiation and longwave radiation was carried out by scaling the diurnal cycles prior to and following the gap. Temperature above the canopy was corrected for the 80 m difference in terrain height by adjusting both temperatures with a constant value, prior to averaging. The constant was equal to plus or minus 0.5 times the average difference between the two temperature records, calculated using the entire dataset. Missing data were interpolated similarly to the radiative forcing. Wind speed was averaged per direction U and V separately.
The precipitation forcing was aggregated from a combination of the MESONET data, up to 10 rain gauges located between #9 and the Fen site in the Sapochi river basin (data collected by R.D. Soulis, see Sellers et al., 1998), and the validation data set (site TF-3, 55.879°N, 98.484°W, elevation 260 m, Northern Old Black Spruce, see below). A weighted averaging procedure was applied by number of used rain gauges as reported. Precipitation on sites #8 and #9 was taken from Belfort weighing gauges when snow depth exceeded 0, and from the tipping bucket gauges otherwise. Tipping bucket on site #8 in 1996 appeared unreliable and was discarded. The Belfort gauges can give (small) negative increments. These were compensated using adjacent time slots. Time slots with no data at all were filled with zero precipitation.
Observations of sensible heat, latent heat, friction velocity and net radiation were observed at the TF-3 old black spruce site (Goulden et al., 1998). This site is already explored during the analysis of Betts et al. (1998), and consists of old Black Spruce, the dominant vegetation type. Additional validation data were snow depth and skin temperature measurements at the MESONET sites. Water equivalent snow depth was calculated from observed snow pack height observations by adopting the snow density formulation by Douville et al. (1995).

3.1.5 Garderen

The Garderen site is a dense Douglas fir forest location in the Speulderbos, in the centre of the Netherlands (52.25°N, 5.68°E; Bosveld, 1997). A continuous record of quality-checked and gap filled meteorological data was available for 9 months in 1989. Data were collected at a 36 m tower in the centre of a patch of moderately homogeneous forest. Wind direction determined the length of homogeneous fetch, and was used to cancel out unrepresentative flux measurements. Roughness length and displacement height are found to be slightly wind speed dependent. Leaf area of the stand varied somewhat thoughout the year, but on the average was very high ($LAI \approx 10$ m^2 m^{-2}).
Flux measurements were carried out using eddy-correlation equipment. This yielded a nearly continuous record of sensible heat flux, but latent heat flux eddy-correlation data are often missing due to equipment failure. A continuous record of latent heat flux has been constructed by filling gaps with energy balance closure residuals.

Table 3.1. Surface characteristics for each site (After Van den Hurk et al., 2000).

parameter	units	Cabauw	FIFE	ARME	BOREAS	Garderen
start date	yymmdd	870101	870501	830901	940118	890401
end date	yymmdd	871231	891108	851001	961130	981231
latitude	°N	51.97	39.029	-3.089	55.879	52.25
longitude	°E	4.93	-96.67	-60.187	-98.484	5.683
z	m	20	2	18	9.33	18
z_{0m}	m	0.284	0.102	1.730	1.241	2.000
z_{0h}	m	0.028	0.010	0.173	0.124	0.200
area fraction H	-	0.384	0.113	0.916	0.992	1.000
area fraction L	-	0.616	0.887	0.084	0.008	0.000
veg. type H	-	19	19	6	3	3
veg. type L	-	1	7	2	17	1
plant type H	-	C3	C3	C3	needle	needle
plant type L	-	C3	C4	C3	C3	C3
veg. Fraction	-	0.90	0.72	0.98	0.90	0.90

3.2 Results

3.2.1 Cabauw

In figure 3.1 the 10-day averaged (daytime) difference of sensible and latent heat flux between the control run and A-gs run are shown for Cabauw. In all figures shown here and in the next sections, the turbulent fluxes of sensible and latent heat are negative upward. From the model output it can be seen that in general the latent heat flux has increased and the sensible heat flux has decreased. From this figure the effect of the canopy conductance on the partitioning of the available energy over the sensible ant latent heat flux becomes clear.
The energy needed for the increase in latent heat mainly comes from the decrease in sensible heat. The largest differences occur in the summer with differences up to 100 W m^{-2}. The soil heat flux and the radiation terms (including the net radiation) are hardly effected by the A-gs model.
In figures 3.2 and 3.3 scatter plots are given of the daily averaged latent heat flux of the control run (figure 3.2) and the A-gs run (figure 3.3) against observations. The thin diagonal line represents the 1:1 line. The heavy diagonal line is a regression line to indicate the bias.

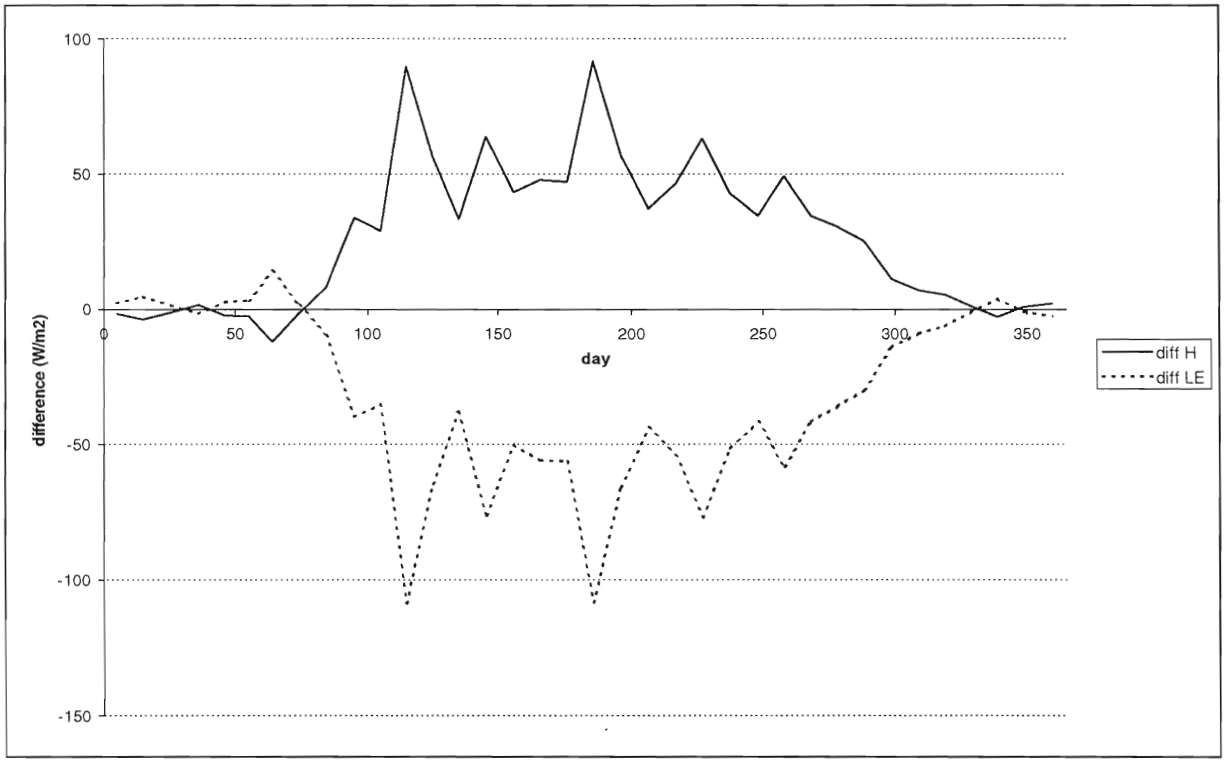

Figure 3.1. 10-day averaged daytime differences (A-gs minus control) in sensible heat flux and latent heat flux. Fluxes are defined negative upward.

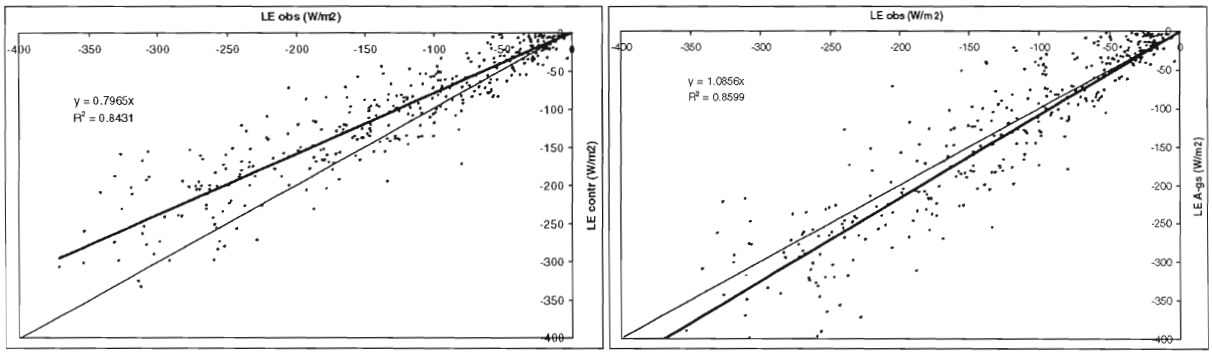

Figure 3.2 and 3.3. Modelled day averaged latent heat flux of the control run and A-gs run compared with observations. Tine line: 1:1; thick line: best fit.

Only observed negative daily averaged values are given, because the greatest effect is expected during daytime. Although the scatter is quite large, it can be seen that on average the A-gs run has a better performance than the control run. The mean error of the control run is –20%, while the mean error of the A-gs run is 9%.
In figures 3.2 and 3.3 R^2 is given also. This is variance in the model output explained by the variance in the observations. It should be stressed that sometimes these values are not realistic and in some cases can be smaller than zero (see for example section 3.2.3). The reason for this is the forcing of the regression line through the origin. In table 3.2 the right values are given. For more details about R^2 see appendix II.
The large scatter in figures 3.2 and 3.3 cannot be explained only by a deficiency in the canopy conductance computation. When the control run and the A-gs run are compared (figure 3.4), the scatter is not as large, so another effect causes the scatter.
Mentioned earlier, the net radiation has barely changed by the A-gs model. The analysed data showed an almost perfect 1:1 relation between the control run and the A-gs run. Only the

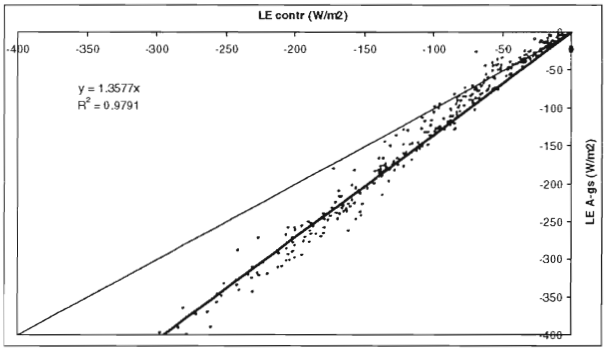

Figure 3.4. Modelled daily averaged latent heat flux of the control run compared with the A-gs run.

partitioning of the available energy has changed. This effect also applies to the other sites, so it will not be mentioned there anymore.
Figure 3.5 shows the cumulative evaporation through the year 1987 for Cabauw. A remarkable fact is that the control run has a better agreement with the observations than the A-gs run. This is not consistent with figure 3.3, from which it would be expected that the cumulative evaporation of the A-gs run should have a better agreement with observations than the control run.

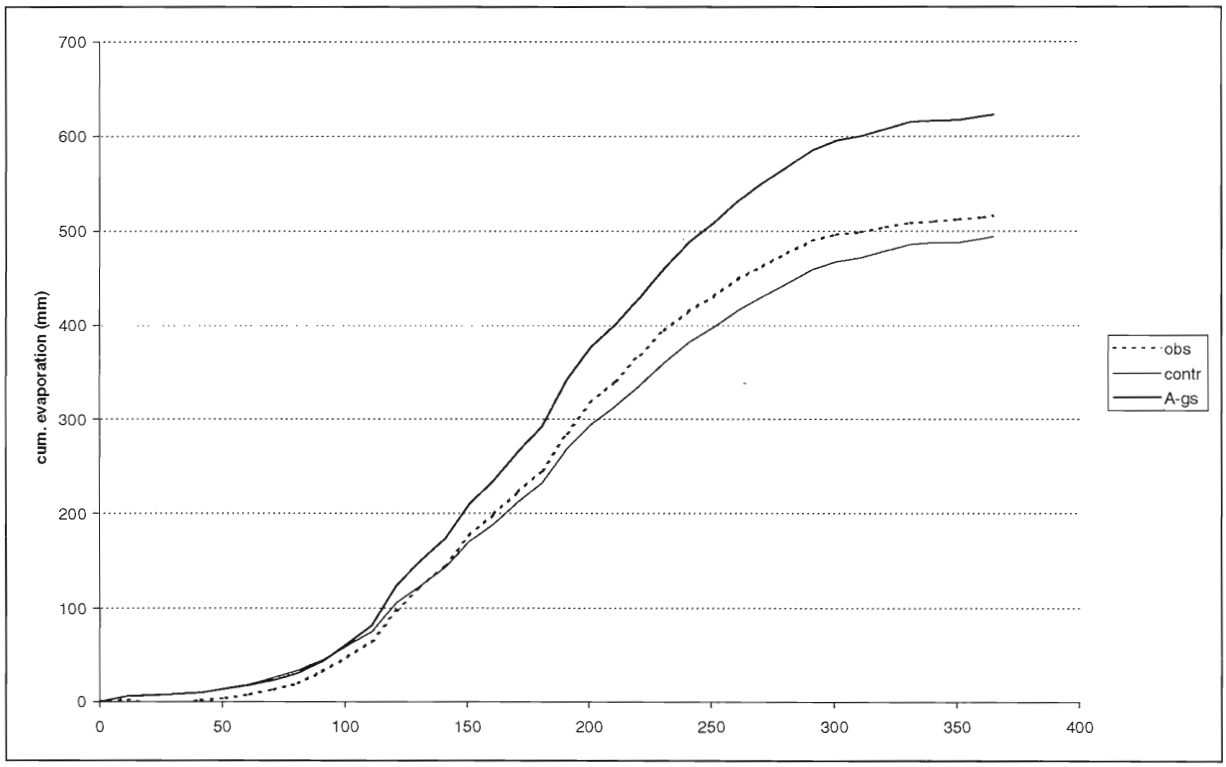

Figure 3.5. Cumulative evaporation in 1987 for the Cabauw site, using whole day averaged latent heat fluxes.

In figure 3.6 again the cumulative evaporation is given, using the same data as in the previous figure but only considering daytime observations of latent heat (here $LE_{obs} < 0$). From this figure it can be seen that in both model cumulative evaporation has not changed, i.e. $LE_{mod} > 0$ is not simulated. By excluding the nocturnal observations of latent heat, the observed cumulative evaporation has increased. The modelled nocturnal latent heat fluxes are

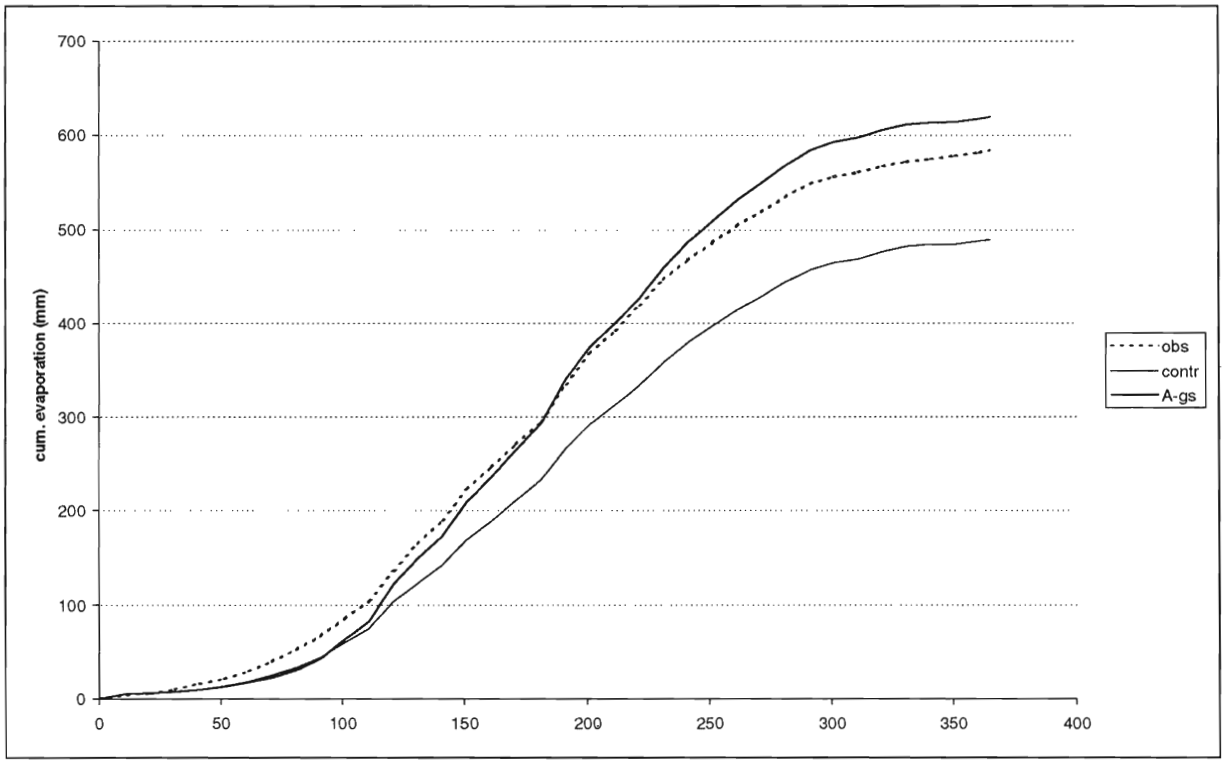

Figure 3.6. Cumulative evaporation in 1987 for the Cabauw site, only using daily averaged latent heat fluxes less than zero.

approximately zero (i.e. no dewfall), which is not realistic. The JS calibration compensates for the fact that $LE > 0$ is not simulated. One has to be cautious by comparing modelled cumulative or averaged fluxes over a day or a year with observations.
For the 3D validation this effect cannot be quantified for the reason that no observations of cumulative evaporation are available for the entire European continent. Only (relative) differences between the control run and the A-gs are made visible (see section 4.1.3).

3.2.2 FIFE

In figures 3.7 and 3.8 the daily averaged daytime (2 hours around local noon) latent heat flux is compared with observations for days 147 till 289 of FIFE (end of May till mid October). Figure 3.7 shows the control model, figure 3.8 shows the A-gs model. As for the Cabauw site the mean error for the A-gs model is smaller than that for the control model, respectively 5% and -12%. The scatter is somewhat larger than for Cabauw.

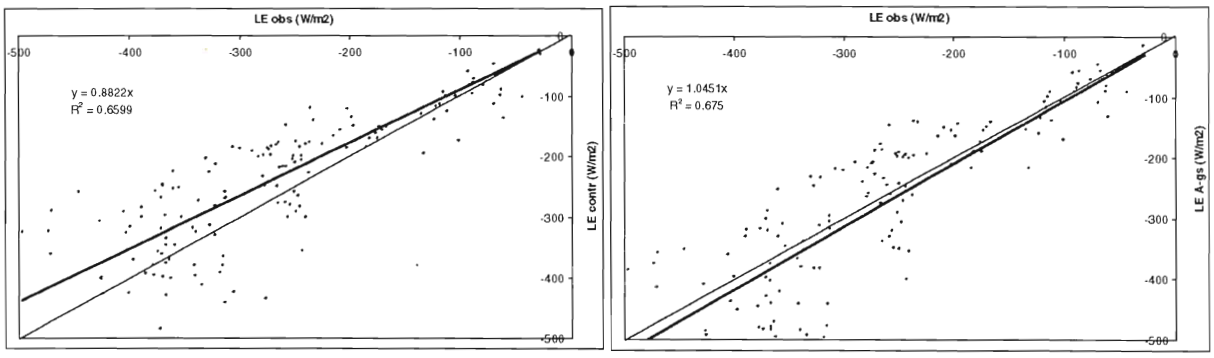

Figures 3.7 and 3.8. Modelled daily daytime averaged latent heat flux of the control run and A-gs run compared with observations.

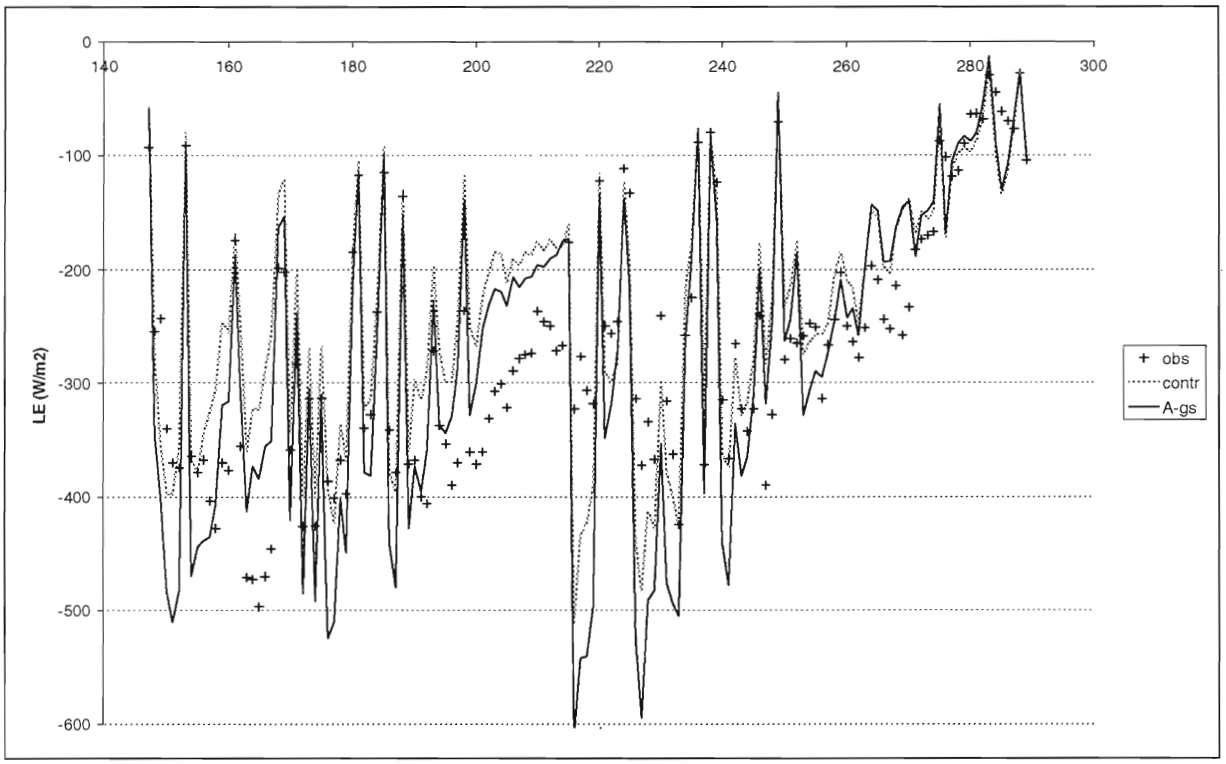

Figure 3.9. Daily averaged daytime latent heat flux for the FIFE site.

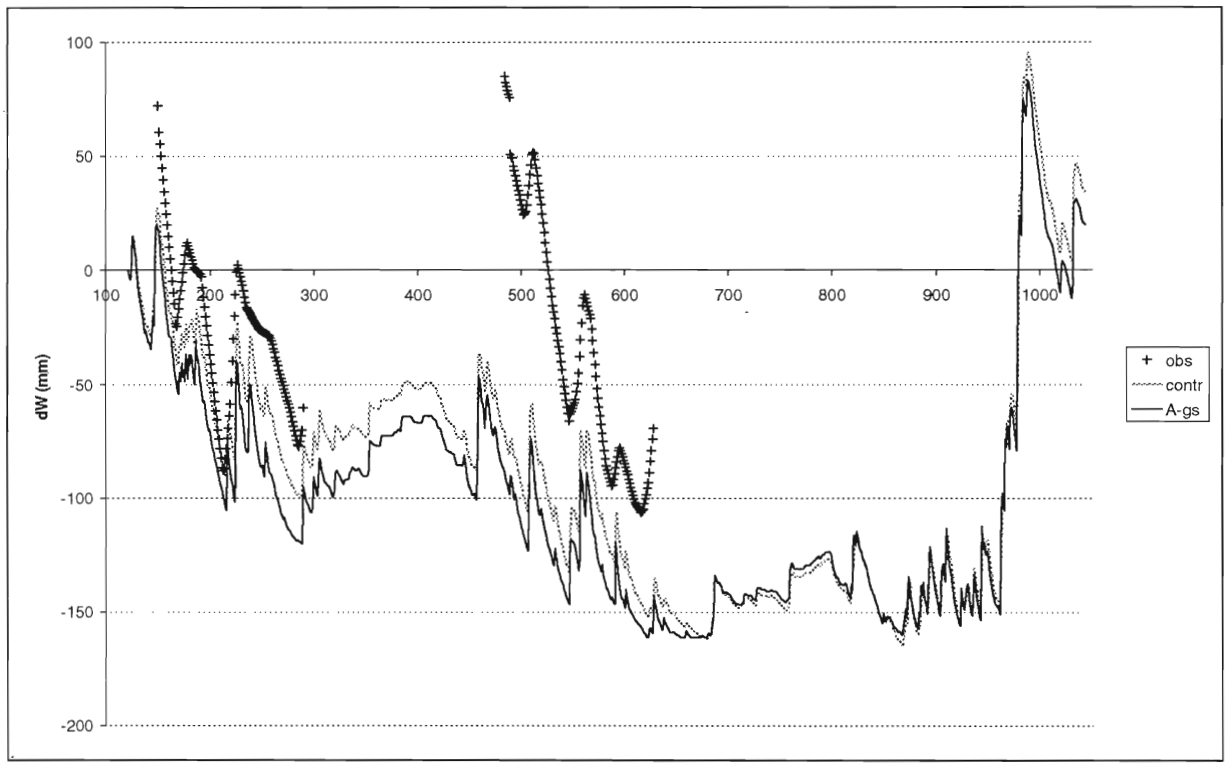

Figure 3.10. Cumulative soil moisture change in the total soil volume relative to the initial profile.

In figure 3.9 the daily averaged daytime latent heat flux is shown for day 147 till 289. According to figure 3.9, the scatter in both figures 3.7 and 3.8 is caused by a deficiency in both models. From about the 15th July (day 195) untill 1st August 1987 (day 215) a very dry period occurred. Both models do not compute this dry period correctly, but the control model

underestimates the latent heat flux for very dry conditions more than the A-gs model. This also can be seen in figures 3.7 and 3.8.
For the FIFE data set soil moisture measurements are available also. In figure 3.10 the change of soil water in the total 2.89 m soil column relative to the initial profile is shown. In 1987 more water is extracted from the soil the A-gs model than by the control model. Not seen is this picture is that the difference in total soil moisture between the A-gs model and the control model is about 100 mm and more or less constant in time. A typical feature of the A-gs model is that the evaporation is less effected by soil moisture stress (see figure 3.9, where the evaporation is larger for the A-gs run). This can be attributed to the modified soil moisture stress function (see section 2.2).

3.2.3 ARME

In figures 3.11 and 3.12 the daily averaged daytime latent heat flux is shown for the ARME data set. A large scatter can be seen in both figures. For the control run, even no correlation between the observations and the model output is given. A negative R^2 is seen, which is not realistic (see page 17). There is some correlation for the A-gs run.

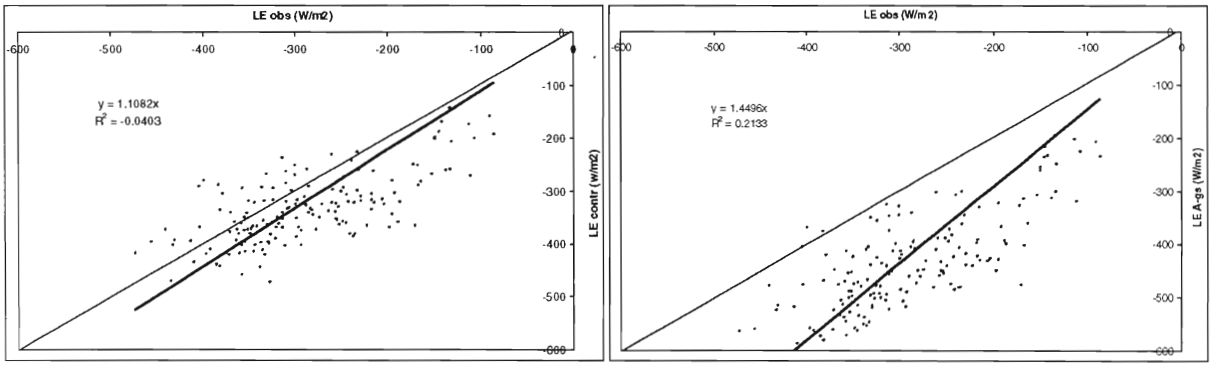

Figures 3.11 and 3.12. Modelled daily daytime averaged latent heat flux of the control run and A-gs run compared with observations.

As for Cabauw and the other sites, the large scatter is not only due to a deficiency in the model. Here, also incorrect measurements of latent heat flux may be a possible reason for the bad correlation. Comparing the modelled fluxes to each other in figure 3.13, the scatter is not as large as in figures 3.11 and 3.12.

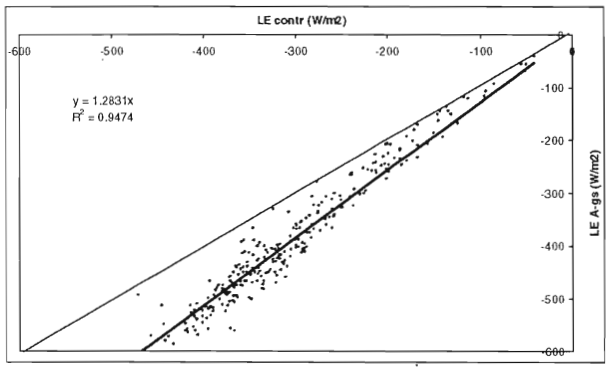

Figure 3.13. Modelled daily averaged daytime latent heat flux of the control run compared with the A-gs run.

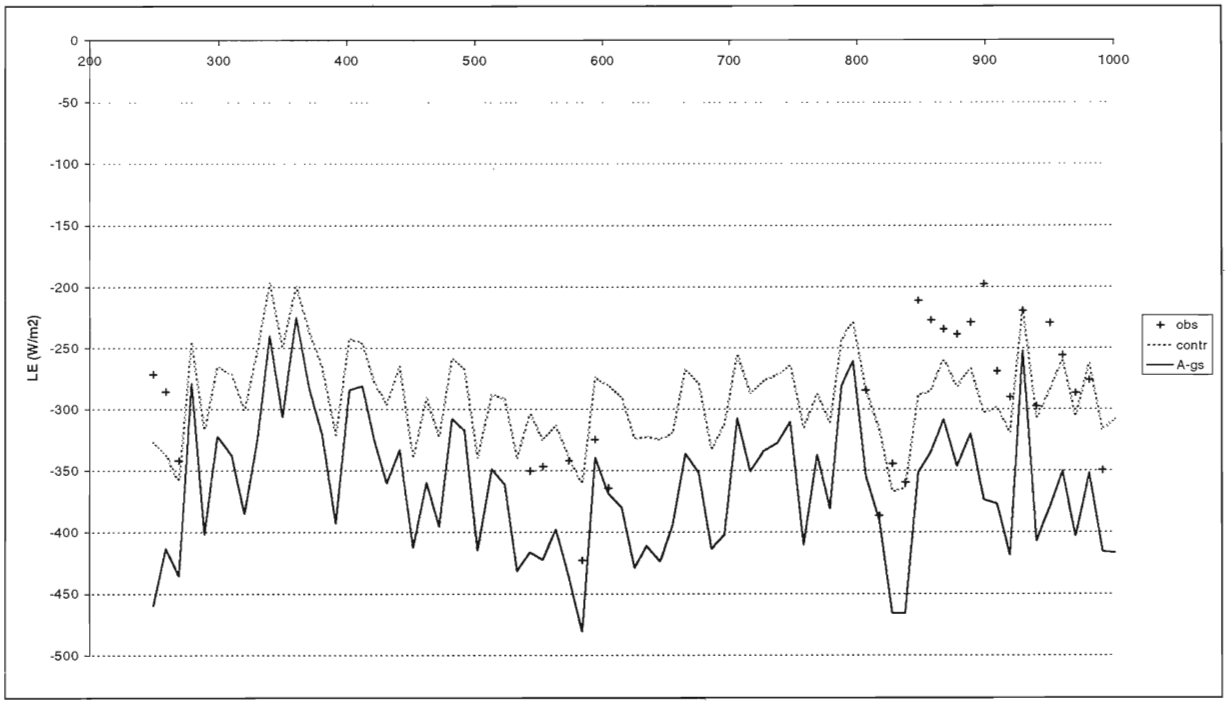

Figure 3.14. 10-day averaged daytime latent heat flux for the ARME site.

In figure 3.14 the 10-day averaged daytime latent heat flux is shown for the ARME measurement period. As in figures 3.11 and 3.12, both runs do not correlate much with observations and the A-gs model evaporates significantly more than the control run.
The A-gs model overestimates the latent heat flux with approximately 45%, which is very high. Excluding days with rain does not improve the results. Both models model the sensible heat very badly. An enormous scatter is shown. Due to the relative low sensible heat values, the correlation between the control model and the A-gs model is also very low for the sensible heat flux. The net radiation is modelled correctly.
There was some uncertainty in selecting the vegetation type for the Amazonian rain forest. In general, C3 plants dominate the earth's surface, but C4 plants dominate warm and/or arid areas (tropics and deserts). To investigate the effect of the plant type, two runs, one with C3 plant types and one with C4 plant types, were done. According to figure 3.15, both runs almost gave the same results.

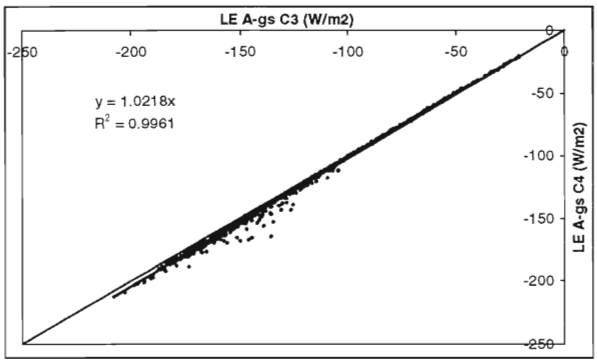

Figure 3.15. Comparison between the modelled latent heat flux for a C3 plant type and a C4 plant type.

Unfortunately no other dataset is available for high broadleaf vegetation. For so far, no adjustments will be made to the model for high broadleaf vegetation. However, based on these results, the A-gs model probably needs some tuning for broad leaf forests. It is expected

the evaporation will be computed too high, but not as much as for needle-leaf forests. A similar choice of parameters as for needle-leaf trees is therefore not recommended.

3.2.4 BOREAS

Three years of daily averaged daytime data of latent heat fluxes are plotted in figures 3.16 and 3.17. The control run has a 15% overestimation of the latent heat flux, while in the A-gs run the overestimation is reduced to 8%. The scatter somewhat increased.

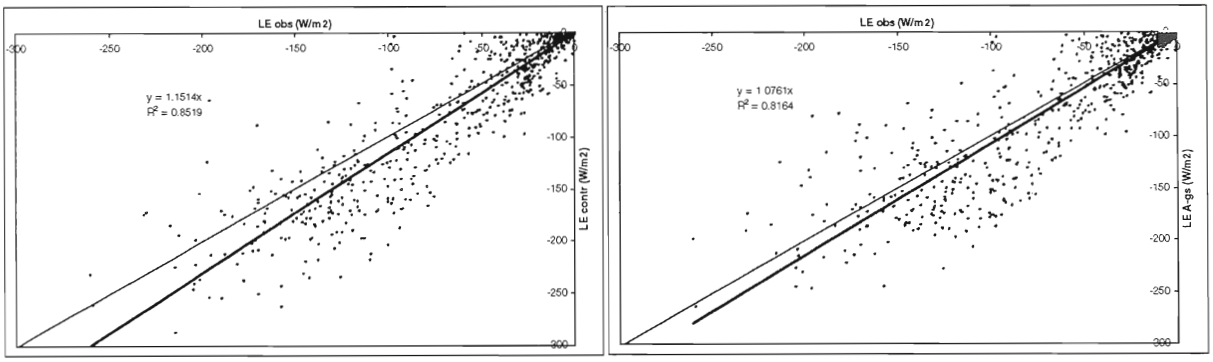

Figures 3.16 and 3.17. Modelled daily averaged daytime latent heat flux of the control run and A-gs run compared with observations.

In figure 3.18 the 10-day averaged daytime latent heat fluxes are given as time series. Compared to the control model, the A-gs model still overestimates the latent heat flux, but the overestimation has reduced, especially during summertime.

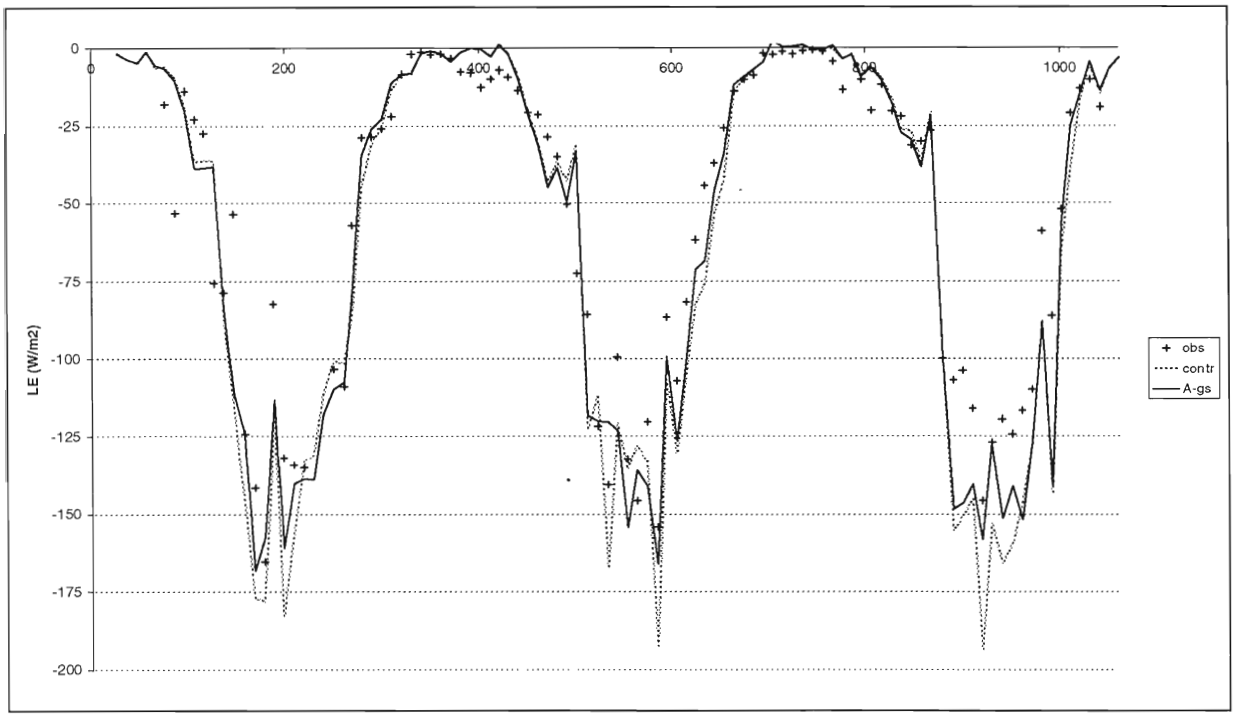

Figure 3.18. 10-day averaged daytime latent heat flux for the BOREAS site.

Both the control and A-gs model underestimate the net radiation by 12%. As can be seen, this deficiency is not caused by a wrong computation of the surface fluxes. Probably wrongly chosen surface characteristics play a role.

3.2.5 Garderen

For the BOREAS site the optimised A-gs model has been proved to be suitable for high needle-leaf vegetation. As an extra validation, the Garderen data is used. As can be seen in figures 3.19 and 3.20, where the modelled daily averaged (daytime) latent heat fluxes are compared with observations, the A-gs model here also computes latent heat fluxes correctly. The mean errors of both models are very small. However, the scatter of A-gs model is larger.

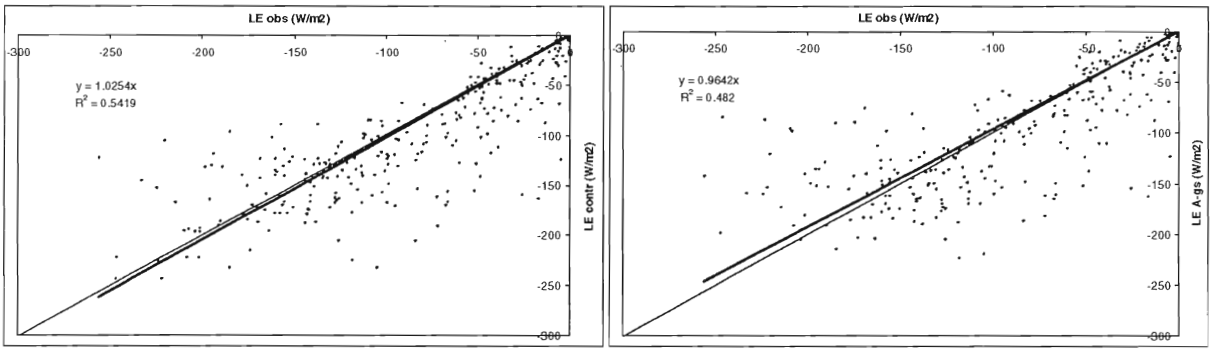

Figures 3.19 and 3.20. Modelled daily averaged daytime latent heat flux of the control run and A-gs run compared with observations.

As for the BOREAS site the 10-day averaged daytime latent heat flux is shown in figure 3.21. Also available are measurements of the sap flow. Because the local characteristics of the site are used in the model runs, the surface may be seen as completely covered with trees. The A-gs model then should describe the sap flow measurement more accurate than the JS model. From figure 3.21, this can not clearly be seen.

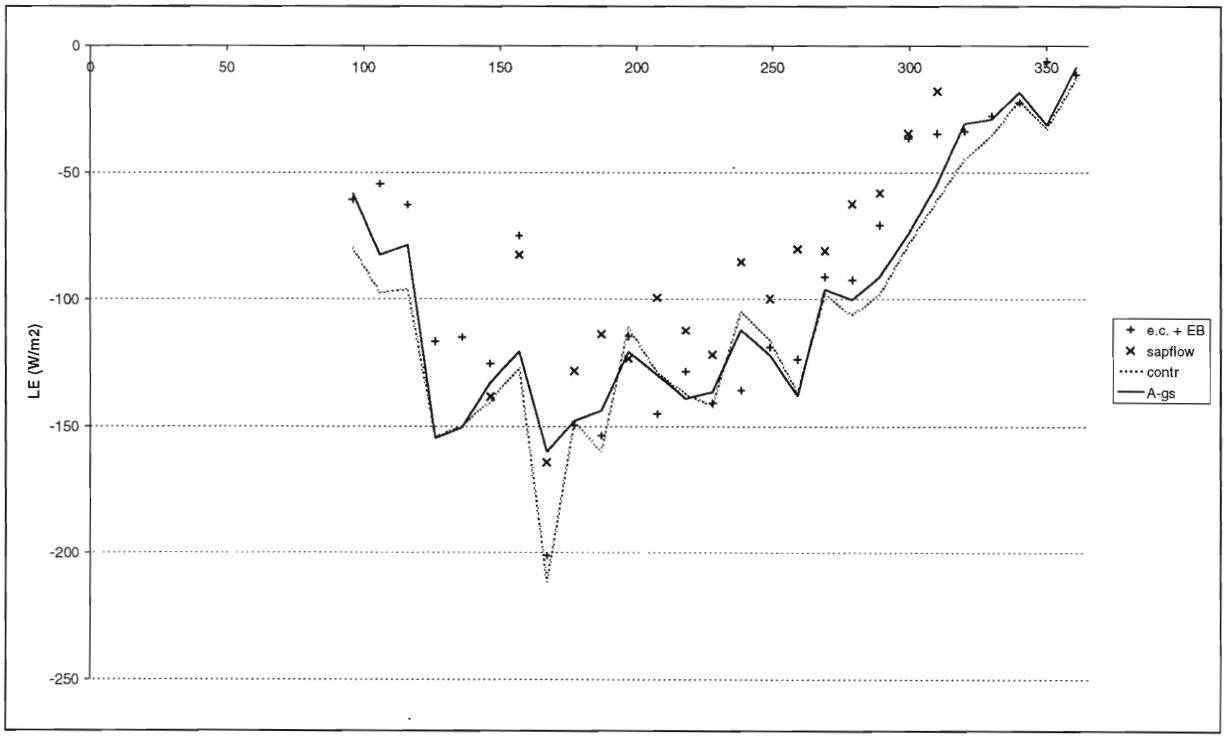

Figure 3.21. 10-day averaged daytime latent heat flux for the Garderen site. e.c. + EB is the latent heat flux obtained with eddy-correlation and the energy balance method. Sap flow is the latent heat flux obtained using sap flow measurements.

3.3 Summary and conclusions

In table 3.2 a summary is given of the mean errors and R^2 values of the latent heat flux, sensible heat flux and net radiation for the different sites. The values are obtained using daily averaged daytime fluxes, as in the previous sections.

Table 3.2. Mean error and R^2 of the latent heat flux, sensible heat flux and net radiation for the different sites.

		Cabauw		FIFE		ARME		BOREAS		Garderen	
		m.e.	R^2	m.e	R^2	m.e.	R^2	m.e.	R^2	m.e.	R^2
LE	contr – obs	0.80	0.84	0.88	0.67	1.11	0.48	1.15	0.85	1.03	0.66
	A-gs – obs	1.09	0.86	1.05	0.68	1.45	0.57	1.07	0.82	0.96	0.59
	A-gs – contr	1.36	0.98	1.19	0.98	1.28	0.92	0.93	0.93	0.94	0.86
H	contr – obs	1.75	0.77	1.33	0.28	0.69	0.06	0.78	0.78	0.85	0.89
	A-gs – obs	1.16	0.63	1.18	0.37	-0.11	0.11	0.80	0.80	0.88	0.89
	A-gs – contr	0.67	0.84	0.87	0.89	-0.05	0.20	1.02	0.98	1.03	0.97
Q^*	contr – obs	1.07	0.98	1.07	0.96	0.95	0.95	0.88	0.90	0.93	0.98
	A-gs – obs	1.09	0.98	1.08	0.96	0.97	0.95	0.88	0.90	0.93	0.98
	A-gs – contr	1.02	1.00	1.01	1.00	1.02	1.00	1.00	1.00	1.00	1.00

For the low vegetation grassland surfaces of Cabauw and FIFE and the tropical forest of ARME the latent heat flux has increased. For the needle-leaf forests of BOREAS and Garderen the latent heat flux has decreased. The scatter for the Cabauw site, FIFE and ARME site somewhat decreased, while for BOREAS and Garderen a small increase is seen.
The sensible heat flux over the low vegetation surfaces has decreased. Over the needle-leaf forests the sensible heat flux somewhat increased. The sensible heat flux computation appears quite bad for the ARME site. The net radiation has increased for the low vegetation surfaces and the tropical forest, while for the needle-leaf forests no change can be seen. The scatter is has not changes for all sites.
The canopy conductance regulates the partitioning of the available energy over the sensible and latent heat flux. Due to the increased evaporation, the skin temperature has decreased, resulting in a small increase in net radiation
For low vegetation surfaces, the A-gs approach certainly has a better performance than the empirical JS approach. The better performance for high vegetation is not as large as for low vegetation. This can be said for both the latent heat flux and sensible heat flux. The adjustment to make the A-gs model suitable for needle-leaf forests has been proved to be quite well, so it can be applied for practical use of the model.
Based on the results in this chapter, it can be concluded that applying A-gs model by Ronda et al. (2001), in general the computation of the surface fluxes has become more accurate, i.e. a smaller mean error and a smaller R^2.

4. 3D validation of the A-gs model

4.1 Setup of the 3D computation

4.1.1 Model configuration

The A-gs model by Ronda et al. (2001) has been implemented in the ERA40 surface scheme (Van den Hurk et al., 2000). This surface scheme is hosted by the Regional Atmospheric Climate MOdel RACMO (Christensen et al., 1996). The RACMO is used as a tool for the development of physical parameterisations for large-scale weather prediction models and climate models. It contains the HIRLAM dynamics (Gustafsson, 1993) and the ECHAM4-GCM physics (Roeckner et al., 1996).
The horizontal resolution of the grid boxes is approximately 50 km and the vertical structure of the RACMO consists of 19 model layers. The model is initialised from the ECMWF analysis starting at 1 March 1995 00 UTC. The numerical time step of RACMO is five minutes and output is generated per six hours. The run stops at 1 November 1995 00 UTC.
At the lateral boundaries, ECMWF analyses are used as forcings at six hours time interval. A relaxation function over ten boundary grid boxes is used to smoothen the influence of the boundary conditions. However inconsistencies between RACMO and ECMWF generated fields are found in this relaxation zone, and therefore bands of ten grid boxes are stripped from the model boundary prior to the analysis. In later RACMO versions the relaxation functions are taken wind direction dependent.

4.1.2 Description of the surface classification and vegetation types

An important feature in the validation of the A-gs model is the surface vegetation coverage. As described in section 2.1, low and high vegetation are treated separately in the ERA40 surface scheme. 20 vegetation types are distinguished: six are classified as high vegetation and 14 are classified as low vegetation. The vegetation types are based on the classification of the BATS surface scheme (Dickinson et al., 1993) as given in the USGS NOAA based global dataset (USGS, 1999).

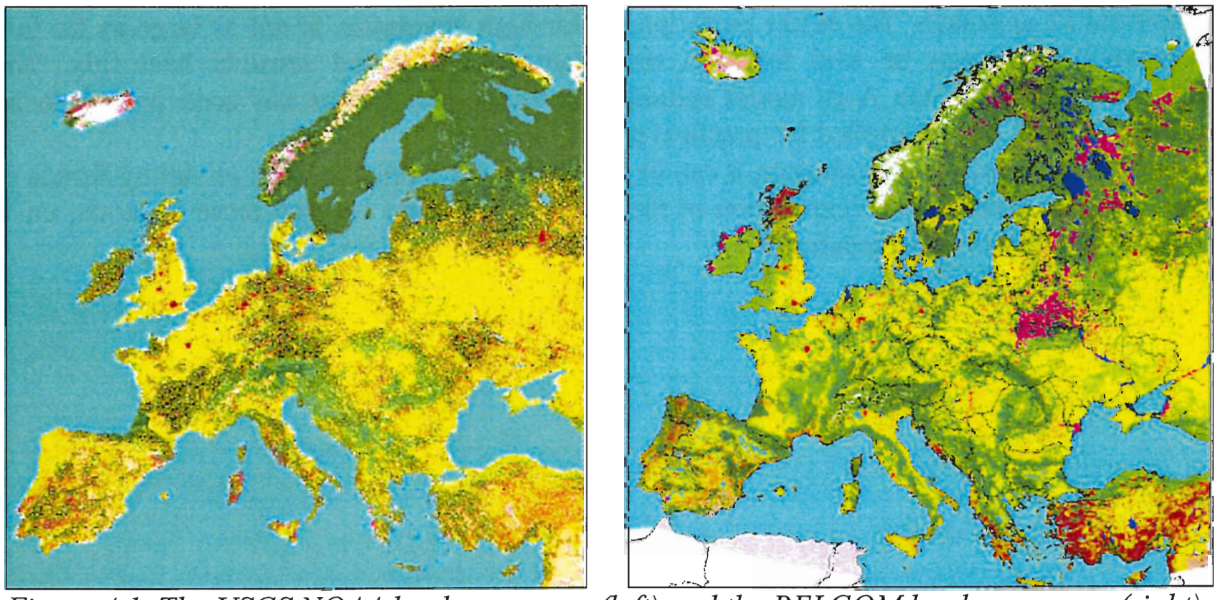

Figure 4.1. The USGS NOAA land cover map (left) and the PELCOM land cover map (right).

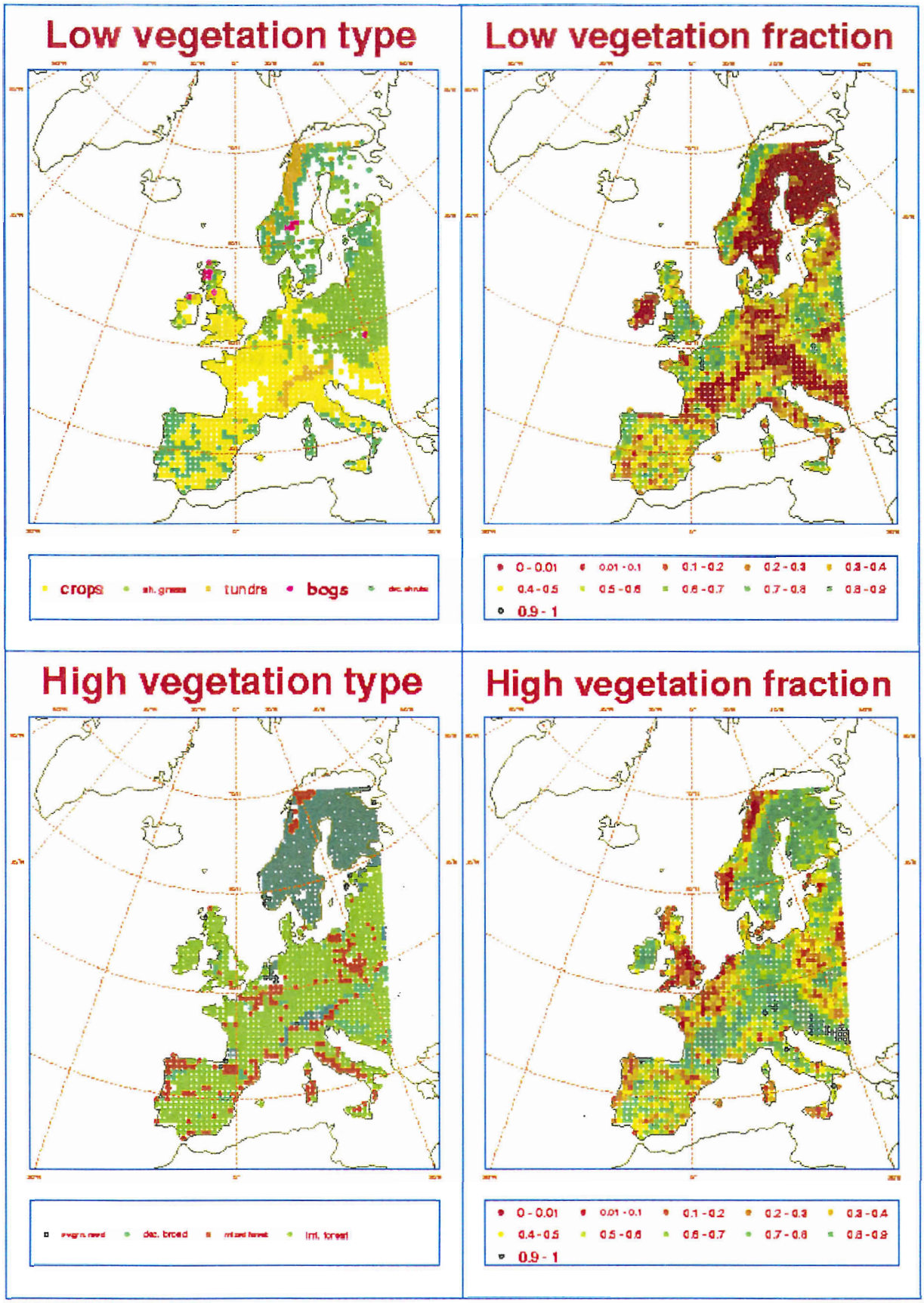

Figure 4.2. RACMO low and high vegetation coverage map, based on the USGS NOAA global dataset.

In figure 4.1 two land cover maps are shown (at slightly different projection). Using these maps, a general picture of the vegetation distribution over the European continent can be obtained. Low vegetation surfaces, dominantly covered with crops and grassland, can be found in Britain, The Netherlands, Belgium, Northwest of France, Poland and Russia. Tundra vegetation is found in Norway. Sweden and Finland are dominantly covered with needle-leaf forests. Needle-leaf forests can also be found in a small area in the Southwest of France and across the Alps. Broad leaf forests can be found only in Yugoslavia and parts of Slovakia and Romania. A great part of Europe, i.e. the Centre of France, Germany and some other countries, is a mixture of forests and low vegetation. This type of surface is characterised as interrupted forest. Finally, Spain, Portugal and Italy are characterised by a mixture of interrupted forest and shrub land.
A remark must be made about Ireland. In the BATS classification Ireland is covered with interrupted forest, while in the PELCOM classification Ireland in covered with grassland and bogs.
For each RACMO grid box one low vegetation type and one high vegetation type is selected, each with its own vegetation coverage. The resulting RACMO vegetation map is shown in figure 4.2. Only nine specific vegetation types are present across Europe.
In the A-gs approach for this study three plant types were distinguished: C3, C4 and needle-leaf plants. For the European continent all vegetation types may be considered as C3 plants. Some crops (such as maize) can be given a C4 label, but for practical reasons this is not done.
Besides the variable vegetation coverage across Europe, also a variable soil map is used (IJpelaar, 2000) which has an impact on the available soil moisture. In figure 4.3 the distribution of soil texture classes is given.

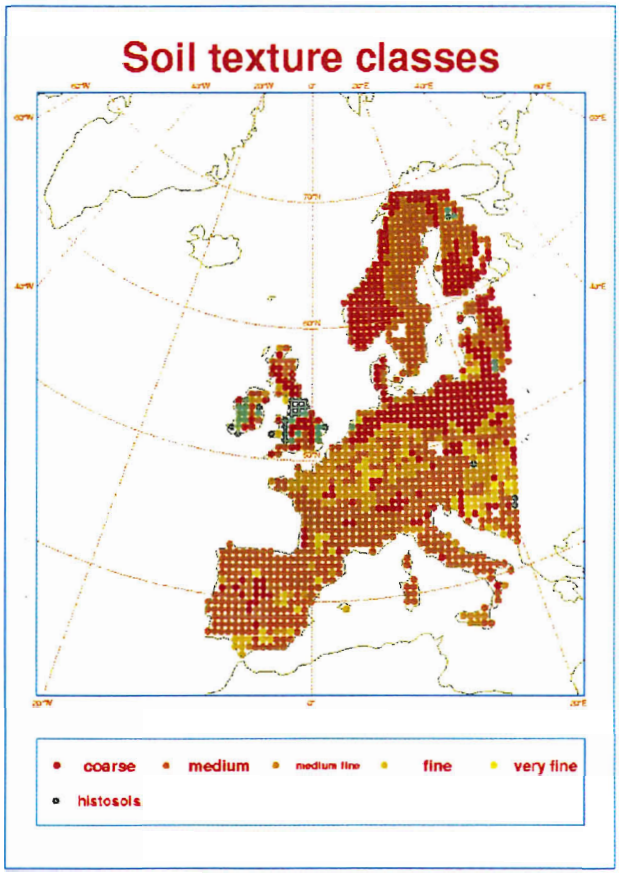

Figure 4.3. RACMO soil texture classes.

Coarse soil textures are found in Norway and in a band reaching from The Netherlands to Russia. Medium soil textures are found in France, Germany and Slovakia. Most of Europe consists of medium texture. In England and Ireland organic histosols can be found.

4.1.3 Analysis setup and description of the regional study areas

Two 3D RACMO runs have been done. The first one is the control run, where the JS-approach is used to compute the canopy conductance. The second one is the A-gs run, where the A-gs approach is used. Both runs were initialised using the same ECMWF analysis and soil conditions. The two runs are compared with each other and with synops observations.
The analysis setup is as follows. First the entire European continent is considered. The main objective is to get insight in the spatial distribution of several relevant quantities. Time series are given of the turbulent fluxes, net radiation and soil heat flux and the hydrological budget terms. Then maps are shown of the spatial distribution of some relevant quantities per season. A disadvantage is that no observations are available of these quantities, so only the A-gs run and the control run can be compared to each other. There are synops observations of 2m relative humidity and temperature. Maps and time series will be given for these quantities as well as the bias and the unbiased root mean square error. The European continent will be called area 0.
Next, three regional study areas will be considered, selected on dominant vegetation type. Area 1 is the area where the low vegetation coverage is larger than the high vegetation coverage. Area 2 is the area where the high vegetation coverage is larger than the low vegetation coverage, but needle-leaf trees (vegetation type 3, see table 2.1) are excluded. This is done because the A-gs model is modified for this type of vegetation. Finally area 3, represents needle-leaf trees (vegetation type 3). A summary is given in table 4.1. In table 4.2 an outline of the relevant quantities and figures is shown per study area. In figure 4.4 the spatial distribution of study areas 1, 2 and 3 is shown.

Table 4.1. Regional study areas. Chv is the high vegetation coverage, Clv is the low vegetation coverage, Thv is the high vegetation type.

Area	Vegetation type	Selection based on
1	low vegetation	$Chv < Clv$
2	high vegetation	$Chv > Clv$ $Thv \neq 3$
3	high vegetation	$Chv > Clv$ $Thv = 3$

Table 4.2. Outline of the figures per study area.

	area 0	area 1	area 2	area 3
time series fluxes	4.5	4.23	4.29	4.35
time series hydrological budget	4.6	4.24	4.30	4.36
map latent heat flux	4.7 / 4.8			
map sensible heat flux	4.9 / 4.10			
map total precipitation	4.11 / 4.12			
map available soil moisture	4.13 / 4.14			
map relative humidity	4.15 / 4.16			
map temperature	4.17 / 4.18			
time series relative humidity	4.19 / 4.20	4.25 / 4.26	4.31 / 4.32	4.37 / 4.38
time series temperature	4.21 / 4.22	4.27 / 4.28	4.33 / 4.34	4.39 / 4.40

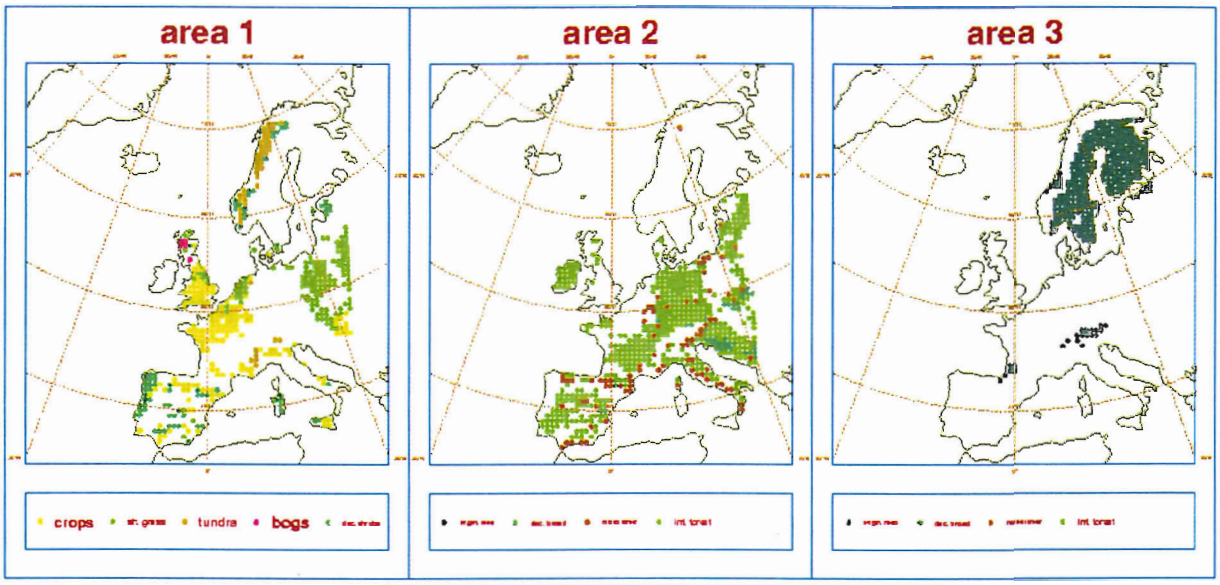

Figure 4.4. Regional study areas. Area 1: low vegetation, area 2: high vegetation (needle-leaf trees excl.), area 3: needle-leaf trees.

A few notes must be made about the figures on the next pages. The time series are 10-day averaged values of the concerned quantities. Thin lines represent the control run and the thick lines the A-gs run. All maps are three-month averages of the concerned quantity. Unless mentioned otherwise, the left picture is the control run, the middle picture the A-gs run and the right picture the difference between the A-gs run and the control run. The fluxes of latent heat and sensible heat are negative upward.
The colouring is as follows: all quantities dealing with moisture (latent heat flux, precipitation, soil moisture and relative humidity are coloured brown (low values) to green (high values). All quantities dealing with heat (sensible heat flux and 2m temperature) are coloured blue (low values) to red (high values). All differences are coloured blue (decrease) to red (increase).

4.2 Results

4.2.1 Study area 0: Europe

In figure 4.5 time series of the sensible and latent heat flux, net radiation and soil heat flux are shown, averaged over the entire European continent. The net radiation and the soil heat flux are barely effected by the A-gs model, while the available energy is redistributed over the sensible and latent heat flux: the latent heat flux has increased and the sensible heat flux has decreased. The largest differences occur in summer. These changes were already noticed in the offline validation.
The effect of the increased evaporation on the hydrological budget can be seen in figure 4.6. Both large-scale and convective precipitation have increased too. The soil has become dryer, implying that the increase in precipitation could not keep up with the increase in evaporation, so the water storage has decreased. Runoff has hardly changed. It can be said that due to A-gs approach the hydrological cycle has intensified.
The initial state of the soil moisture content in the A-gs run was not in equilibrium. Both the control run and the A-gs run were initialised using the same soil conditions. Probably due to the non-equilibrium initial state of the A-gs run, more water is available in the soil, leading to a higher evaporation and a larger decrease of water storage.

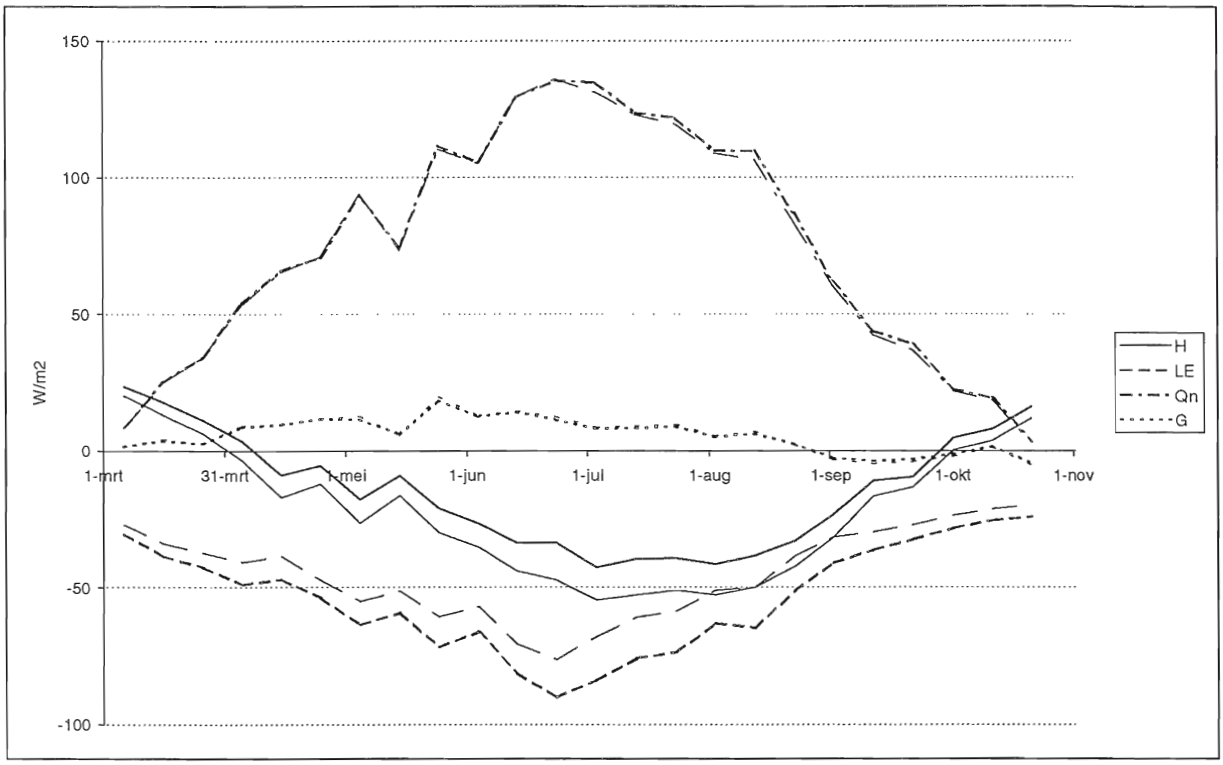

Figure 4.5. Sensible and latent heat flux, net radiation and soil heat flux for the entire study area of Europe. Thin lines: control run. Thick lines: A-gs run.

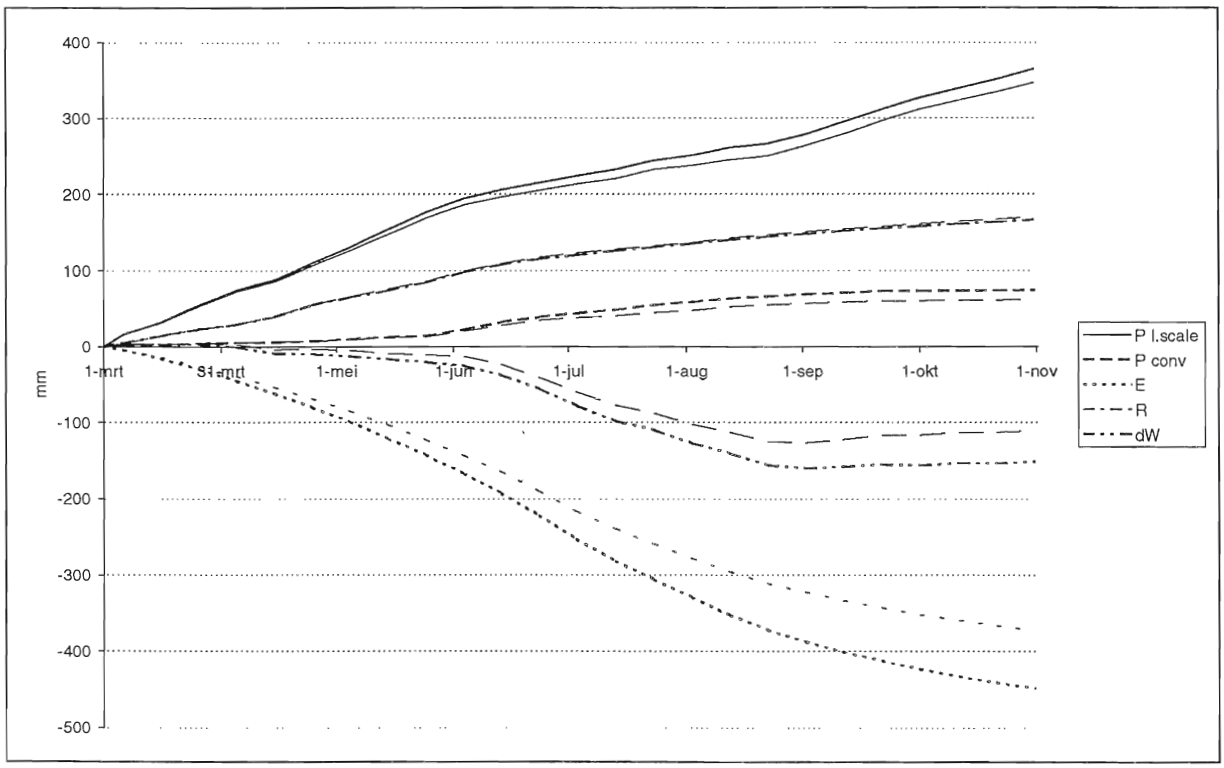

Figure 4.6. Cumulative large-scale (P l. scale) and convective precipitation (P conv), evaporation (E), total runoff (R) and change of soil water storage (dW) for the entire study area of Europe. Thin lines: control run. Thick lines: A-gs run.

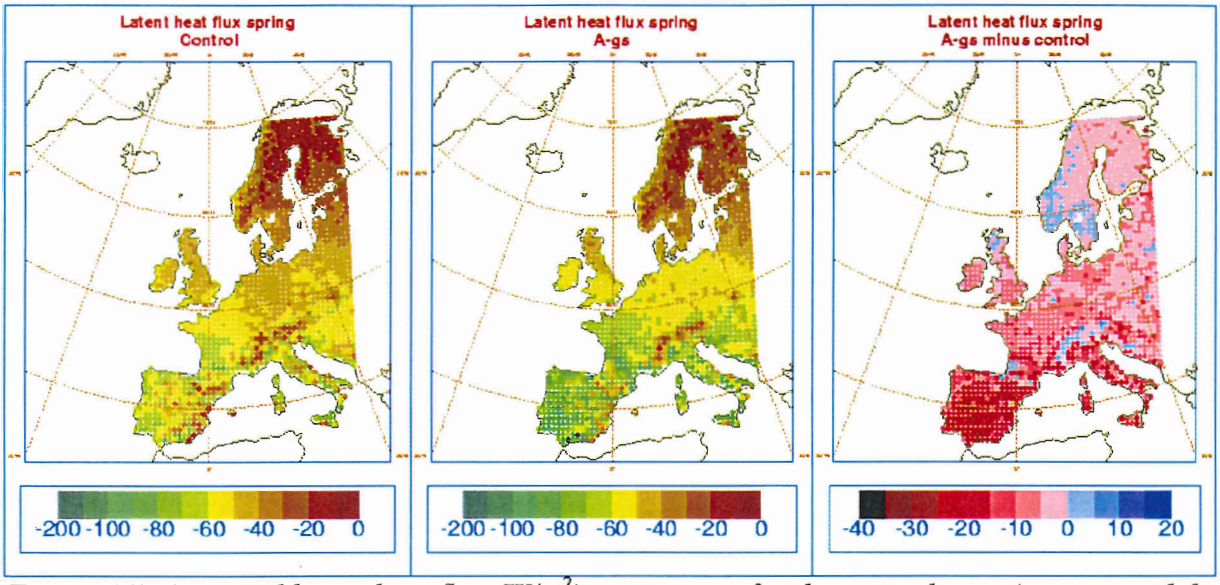

Figure 4.7. Averaged latent heat flux (W/m^2) over spring for the control run, A-gs run and the difference between the A-gs run and control run.

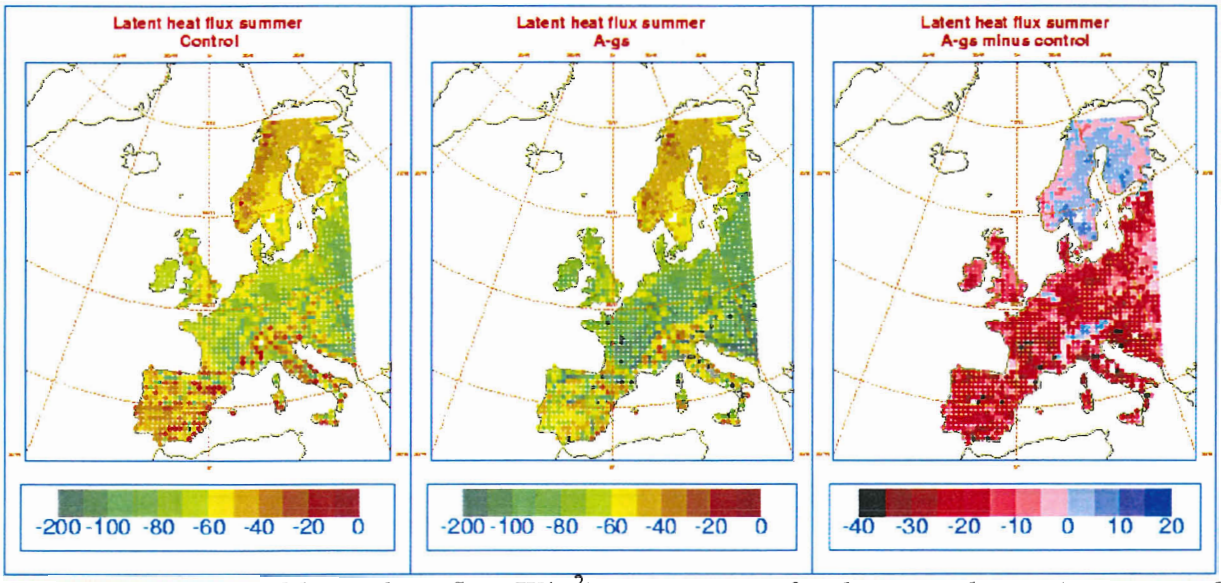

Figure 4.8. Averaged latent heat flux (W/m^2) over summer for the control run, A-gs run and the difference between the A-gs run and control run.

For this study an equilibrium run was not available, making an analysis of the effect of the A-gs model on the equilibrium hydrological cycle impossible. One should be cautious to extrapolate these results to the climatological time scale.
In figures 4.7 and 4.8 the three-month averaged latent heat flux over respectively spring and summer are shown. The main difference between spring and summer is the increased latent heat flux in summer. Also the difference between the two runs has increased (negative numbers in figures 4.7 and 4.8 indicate an increased upward latent heat flux).
From both figures it becomes clear that the latent heat flux has increased for almost the entire continent, except for the needle-leaf tree area's (area 3): Sweden, Finland, Southwest of France and the Alps. Major increases occur in Spain, Central France, Germany, Italy and Yugoslavia. This increase may be attributed to the representation of the vegetation in the A-gs model. From the results of the offline validation for broadleaf forests, it was seen that the A-gs model for this vegetation type gave a large overestimation of the latent heat flux.

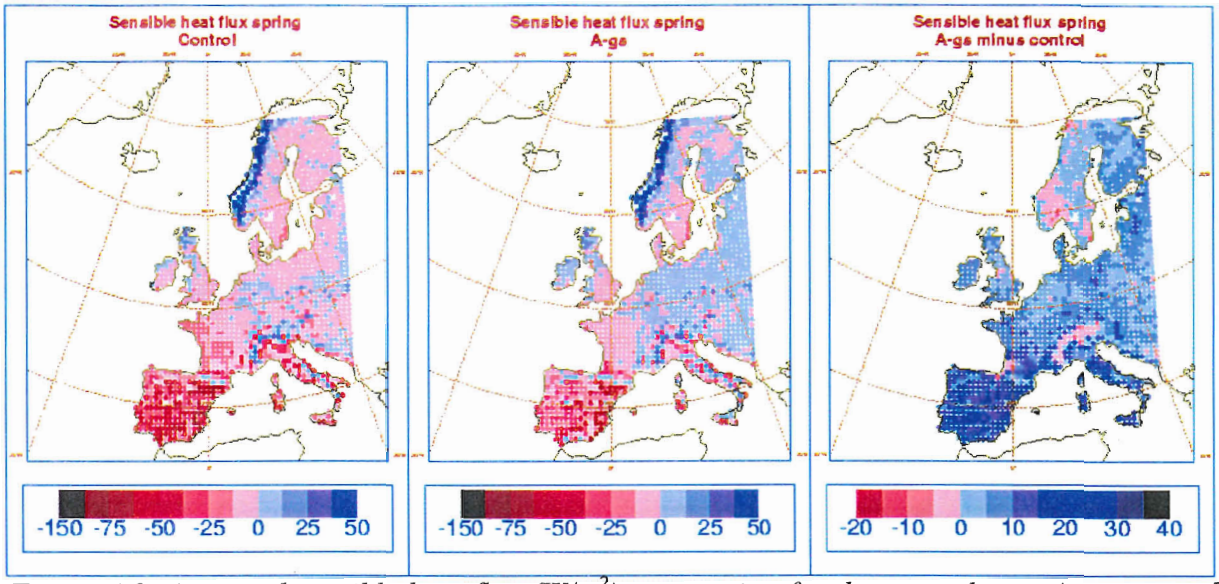

Figure 4.9. Averaged sensible heat flux (W/m^2) over spring for the control run, A-gs run and the difference between the A-gs run and control run.

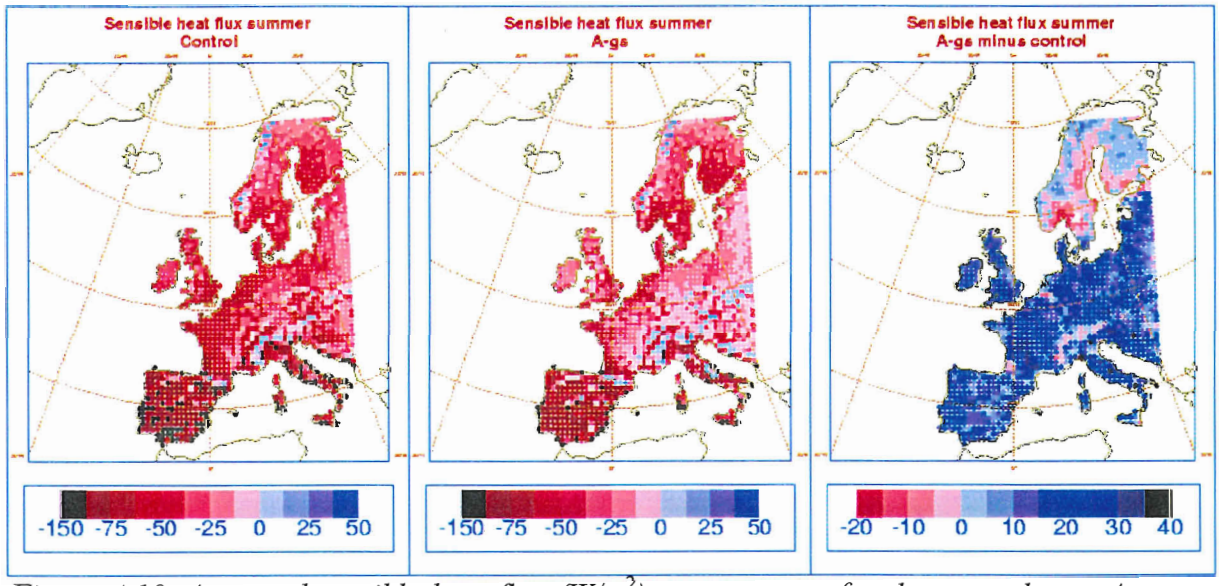

Figure 4.10. Averaged sensible heat flux (W/m^2) over summer for the control run, A-gs run and the difference between the A-gs run and control run.

According to figure 4.2, the areas in Central France, Germany and Yugoslavia are covered with high vegetation of the interrupted forest type (as most of Europe), which is a combination of broadleaf forest and low vegetation. Here the latent heat flux is probably overestimated too. For the low vegetation surfaces (Britain, Holland, Belgium, Western France) the latent heat flux has increased also, but not as much as the high vegetation surface. For areas with needle-leaf forests no change or some decrease can be seen, similar to the results of the offline validation. The reason may lie in the fact that the A-gs model is tuned to the control model for this kind of vegetation. Finally, the increase in Spain and Italy may be a result of the modified soil moisture stress function (2.10). More soil moisture is available for evaporation by applying this modified stress function.
In figures 4.9 and 4.10 the sensible heat flux is shown. In spring typical areas of positive sensible heat fluxes (=downward transport) can be found in Norway and the Alps, probably due to snow coverage on the mountains. Typical high values are found near the coast lines in

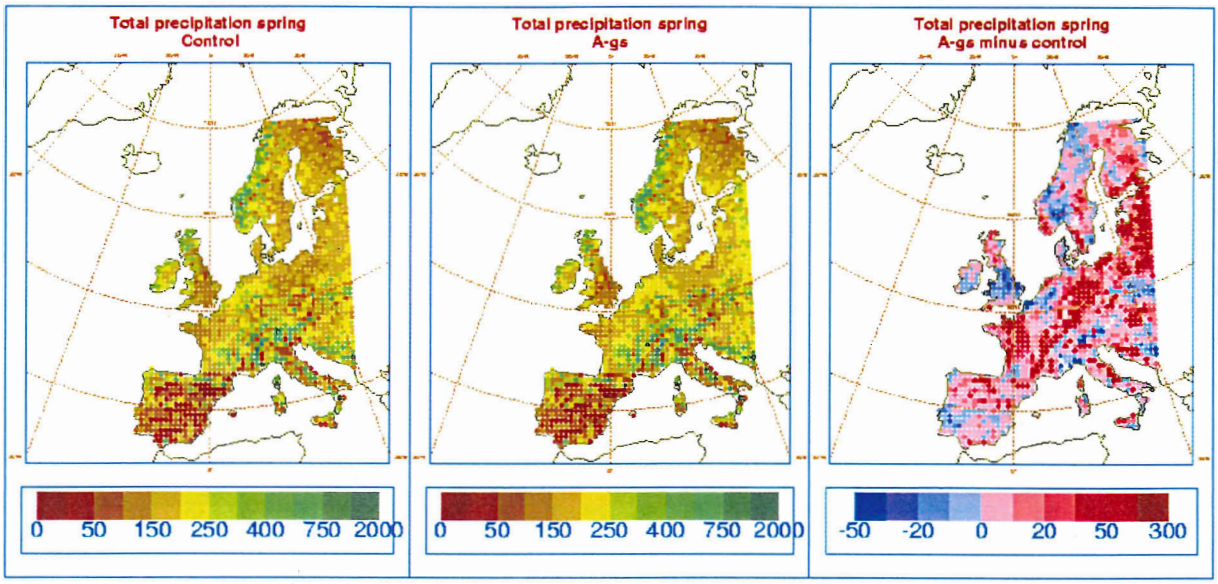

Figure 4.11. Accumulated precipitation (mm) over spring for the control run, A-gs run and the difference between the A-gs run and control run.

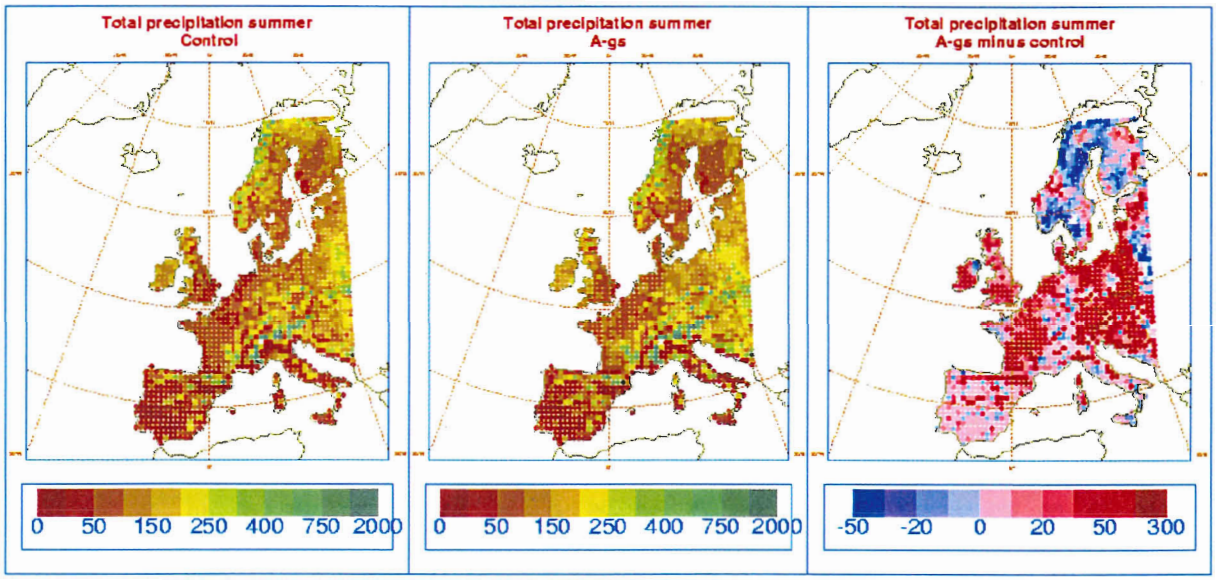

Figure 4.12. Accumulated precipitation (mm) over summer for the control run, A-gs run and the difference between the A-gs run and control run.

summer. As expected, the sensible heat flux has decreased across Europe in both spring and summer. In general the largest differences occur in areas with the largest increase of latent heat. Above the needle-leaf forests the summertime sensible heat flux has somewhat increased.

Figures 4.11 and 4.12 show the accumulated total precipitation over spring and summer. The total precipitation is the sum of the large-scale precipitation (due to large-scale weather systems) and convective precipitation (due to local convection). From figure 4.12 it can be seen that the summer of 1995 was very dry for Western Europe.

The distribution of precipitation across the European continent is similar for both models, although some differences occur. In spring the difference in precipitation is mainly caused by a change in large-scale precipitation. In summer the difference in precipitation in Scandinavia and Britain is caused by a change in large-scale precipitation also. Convective precipitation increases to the east in summer. There is a large increase in convective precipitation above

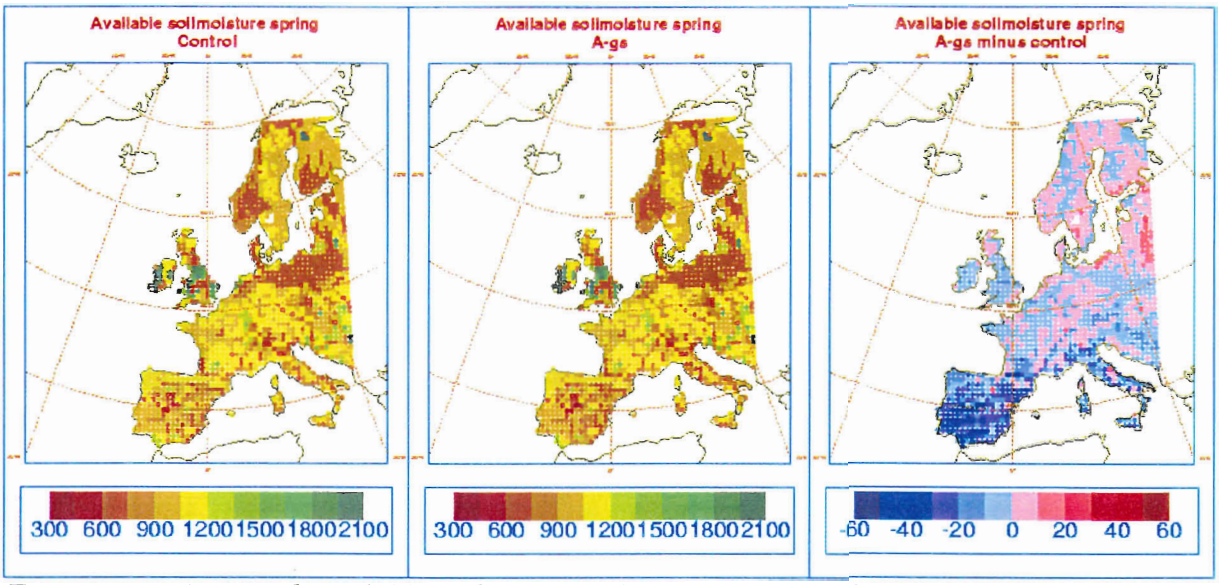

Figure 4.13. Averaged available soil moisture (mm) over spring for the control run, A-gs run and the difference between the A-gs run and control run.

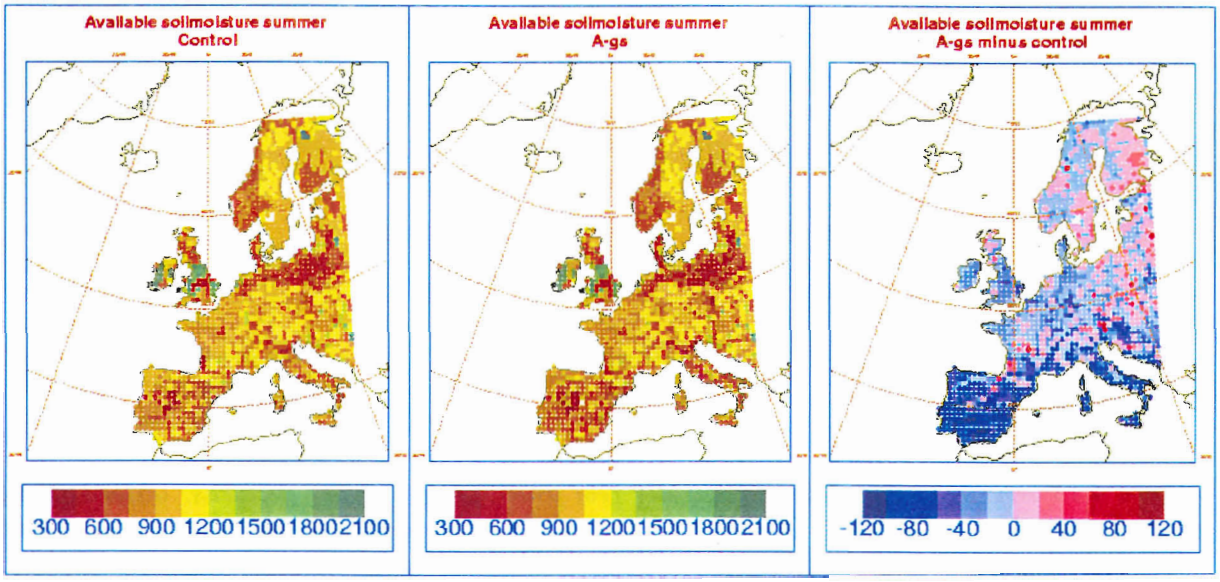

Figure 4.14. Averaged available soil moisture (mm) over summer for the control run, A-gs run and the difference between the A-gs run and control run.

Yugoslavia and surrounding countries. The remaining increase in summer is caused by an increased large-scale precipitation. On average precipitation has increased, except for Scandinavia. The precipitation in Spain is low in the control run and the A-gs run, leading to small differences. A typical band of small differences can be seen over Germany. The larger differences between the two runs can not primarily be assigned to the excessive evaporation over the interrupted forest or broadleaf forest. There is some signal, but over Germany and Spain there is hardly any signal. Other effects must cause the increased precipitation, such as large-scale flows and transport of moisture.

In figures 4.13 and 4.14 the averaged available soil moisture, or soil water storage, is shown. The effect of the variable soil map (figure 4.3) is clear: coarse textured soils contain less water, while histosols contain more water.

In summer the differences between the runs are larger than in spring. Spain, Portugal and Italy have become drier in the A-gs run due to the increased evaporation related to the modified

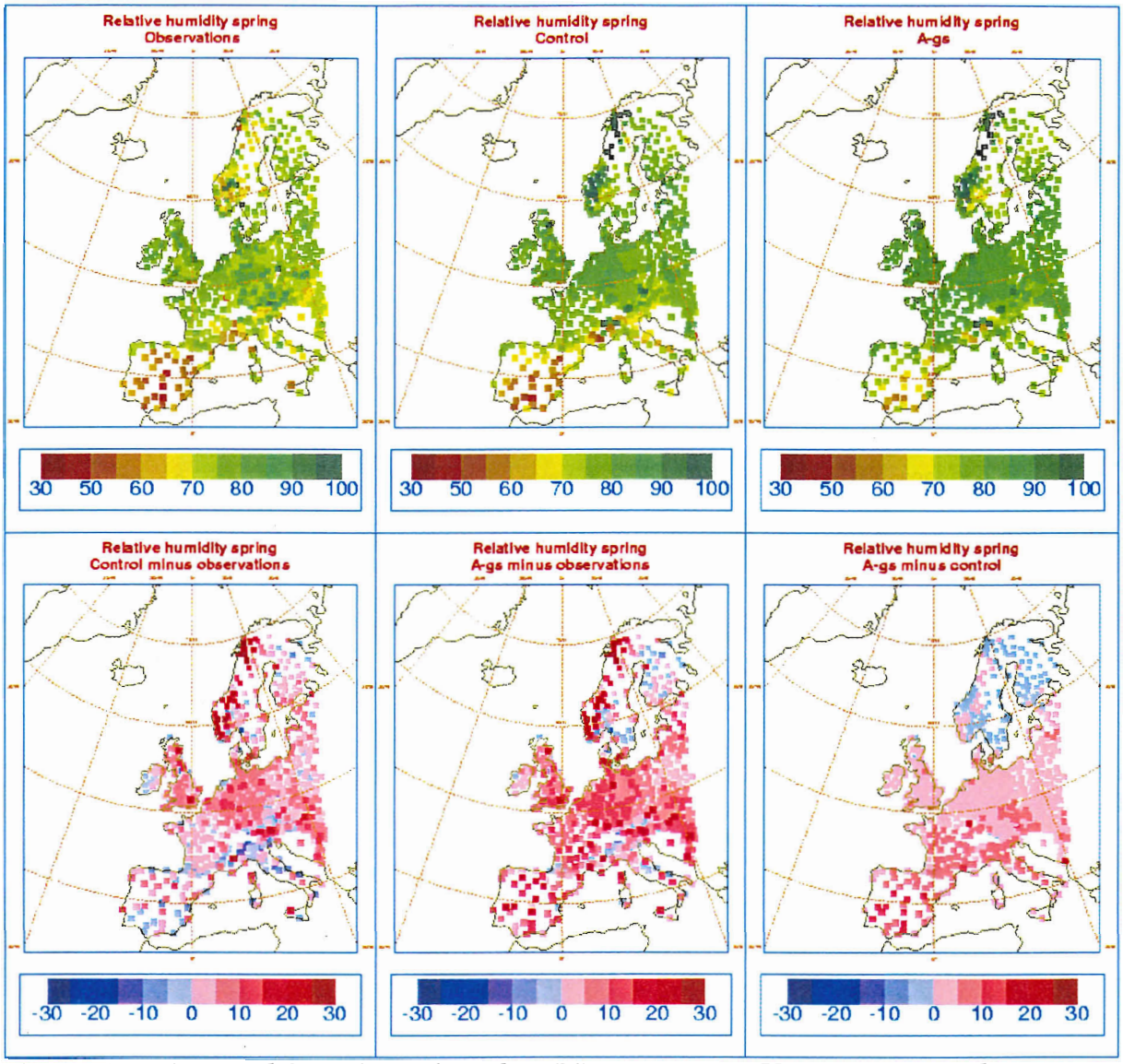

Figure 4.15 Averaged 2m relative humidity (%) over spring. Upper pictures: observations, control run and A-gs run. Lower pictures: differences between the control run and observations, A-gs run and observations and A-gs run and control run.

soil moisture stress function. Also Britain, Holland, Northern France, Germany and Yugoslavia have become drier, but not as much. To the east the available soil moisture has increased. Comparing these figures with the vegetation maps, a weak relation, as for precipitation, with the vegetation types and coverage can be seen: less water is available in areas with high vegetation coverage (area 2) than in areas with low vegetation coverage (area 1). This relation is somewhat disturbed by the variable soil map: histosols show a larger decrease than coarse soils. Also the changes in precipitation influence the available soil moisture, for example in Central France and Germany.

For figures 4.5 to 4.14 no comparison with observations was possible, because no observations are available. However, there are observations of 2m relative humidity and temperature. To compare the model output with observations, the model output is bilinearly interpolated to the specific synops station coordinate, leading to the distribution in figures 4.15-4.18. Fewer observations are available in Portugal and Spain, the Alps, Scandinavia and Bosnia-Herzegovina.

In figures 4.15 and 4.16 the 2m relative humidity is compared with observations. The upper

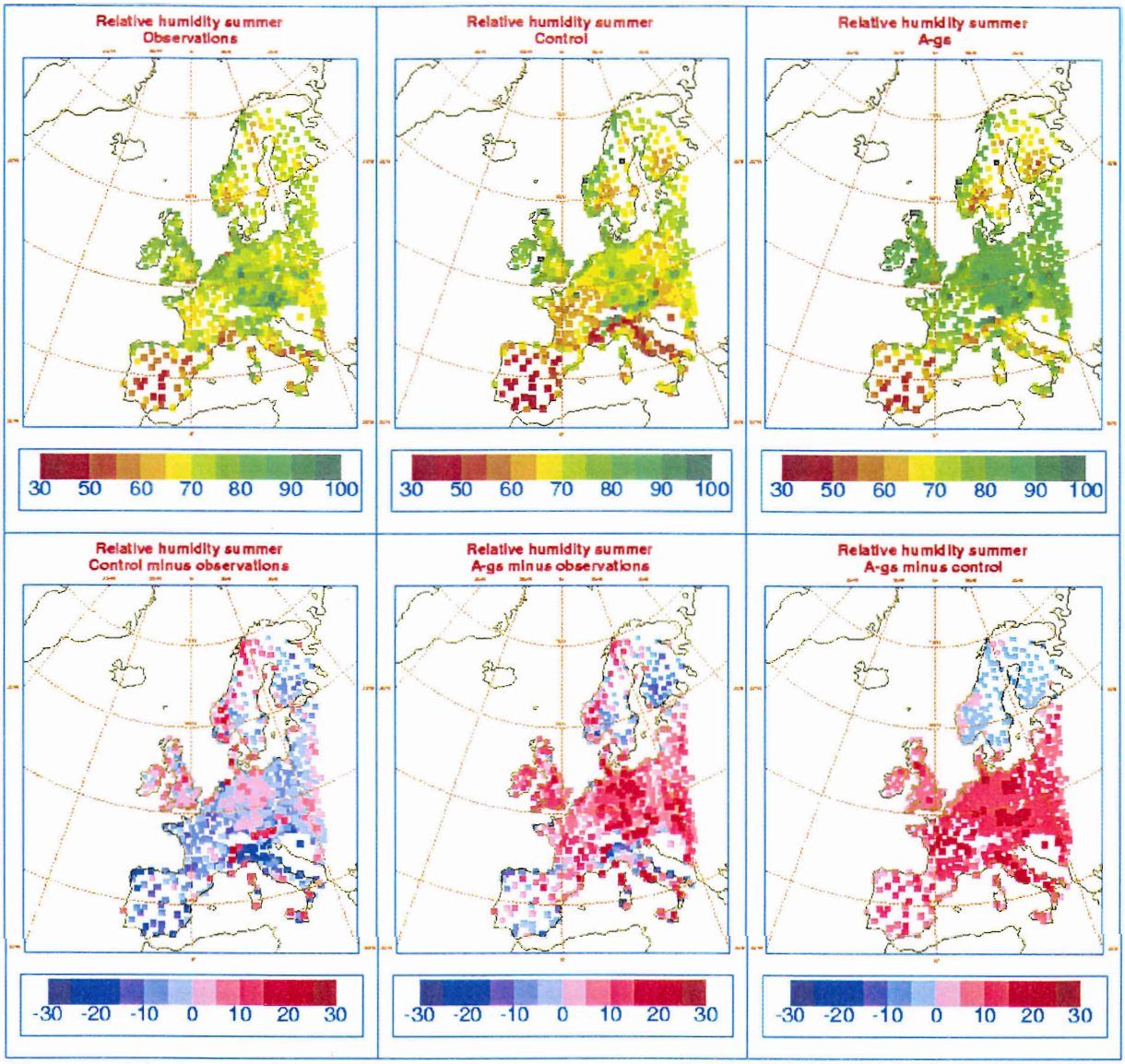

Figure 4.16. Averaged 2m relative humidity (%) over summer. Upper pictures: observations, control run and A-gs run. Lower pictures: differences between the control run and observations, A-gs run and observations and A-gs run and control run.

pictures show the observations and the two model runs, the lower pictures show the differences between the models and the observations. In spring it can be seen that the relative humidity is calculated too high on average by both models. A much too high humidity is calculated above the Norwegian Mountains, probably caused by low temperatures and high precipitation. Also see the figures 4.9, 4.10 (sensible heat flux), 4.11 and 4.12 (precipitation). Except for needle-leaf forests, the relative humidity has increased in the A-gs run.

In summer the relative humidity is calculated too low by the control model, while it is calculated too high by the A-gs model, except for dry areas (Spain and Italy), where the relative humidity is calculated more correctly by the A-gs model. In general it can be seen that for high vegetation surfaces, for example Central France and Germany, the relative humidity is too high, while for low vegetation more correct values are given by the A-gs model.

In figures 4.17 and 4.18 the 2m temperature is compared with observations. Both models show the north-south temperature gradient in spring and summer. This was not seen in the relative humidity. In spring, a weak east-west gradient in the temperature bias can be seen for the control model. Both models show an underestimated temperature over Spain and Central

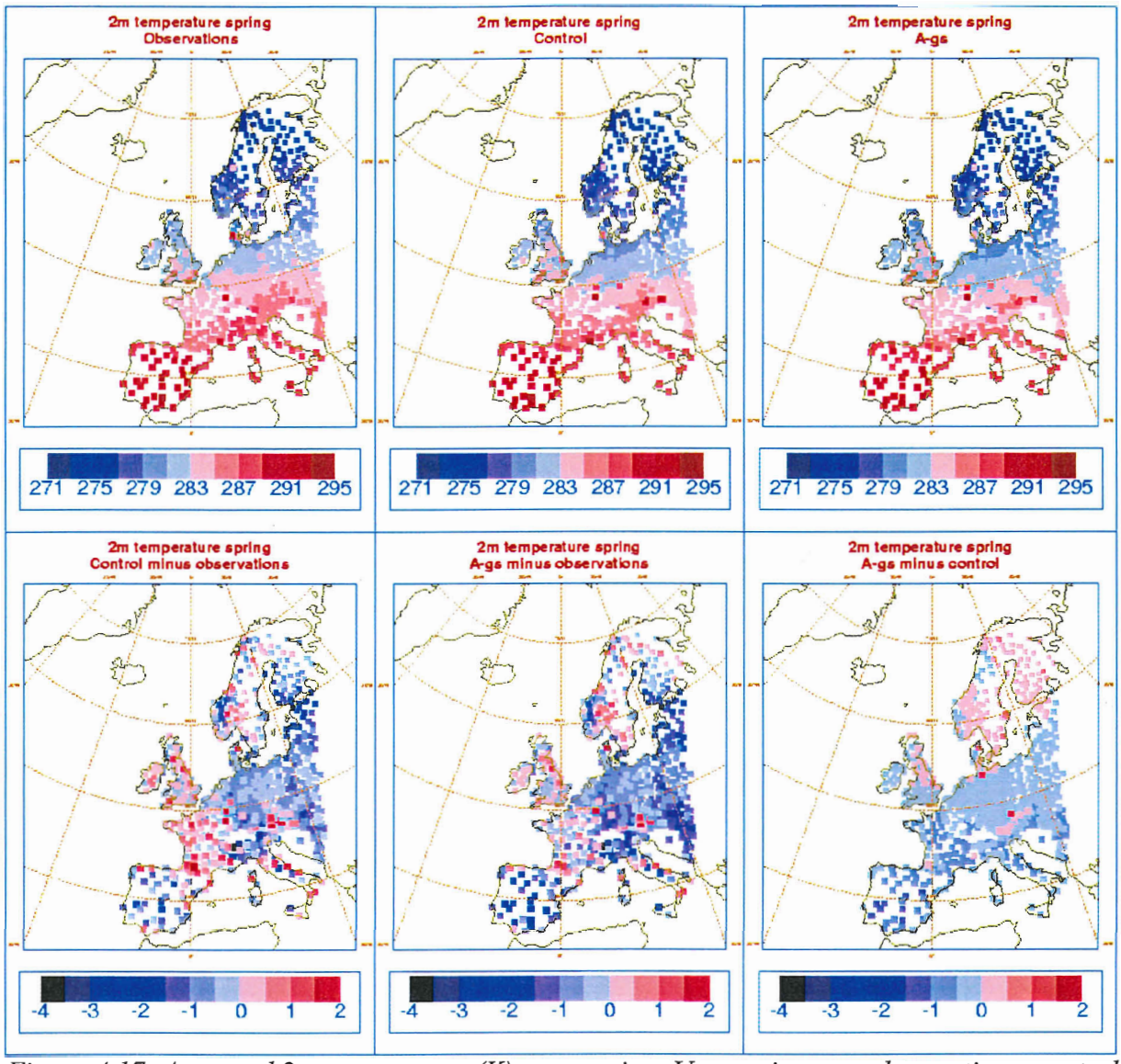

Figure 4.17. Averaged 2m temperature (K) over spring. Upper pictures: observations, control run and A-gs run. Lower pictures: differences between the control run and observations, A-gs run and observations and A-gs run and control run.

Europe in spring, while in summer the temperature is overestimated by the control model. In summer larger differences occur (as for most quantities). Across Central Europe, the control run is too warm, while the A-gs run is somewhat too cold in comparison with the observations. Comparing the A-gs run with the control run, in general a cooling is seen, except for needle-leaf trees.

The following figures 4.19-4.40 will show 10 day averaged time series of 2m relative humidity and temperature compared with observations. For study areas 1 to 3 the energy budget and hydrological budget will be given also. For the 2m relative humidity and temperature first the observations together with the model output will be shown. Then the bias and the unbiased root mean square error (further called RMS) will be shown to get more insight in the performance of both models (see appendix II).

In figure 4.19 the modelled relative humidity is compared with observations for the entire European continent. Low values of relative humidity occur in June, July and August 1995. In spring both models overestimate the relative humidity, while in summer the relative humidity is overestimated by the A-gs model only. In spring and autumn the two model agree with each

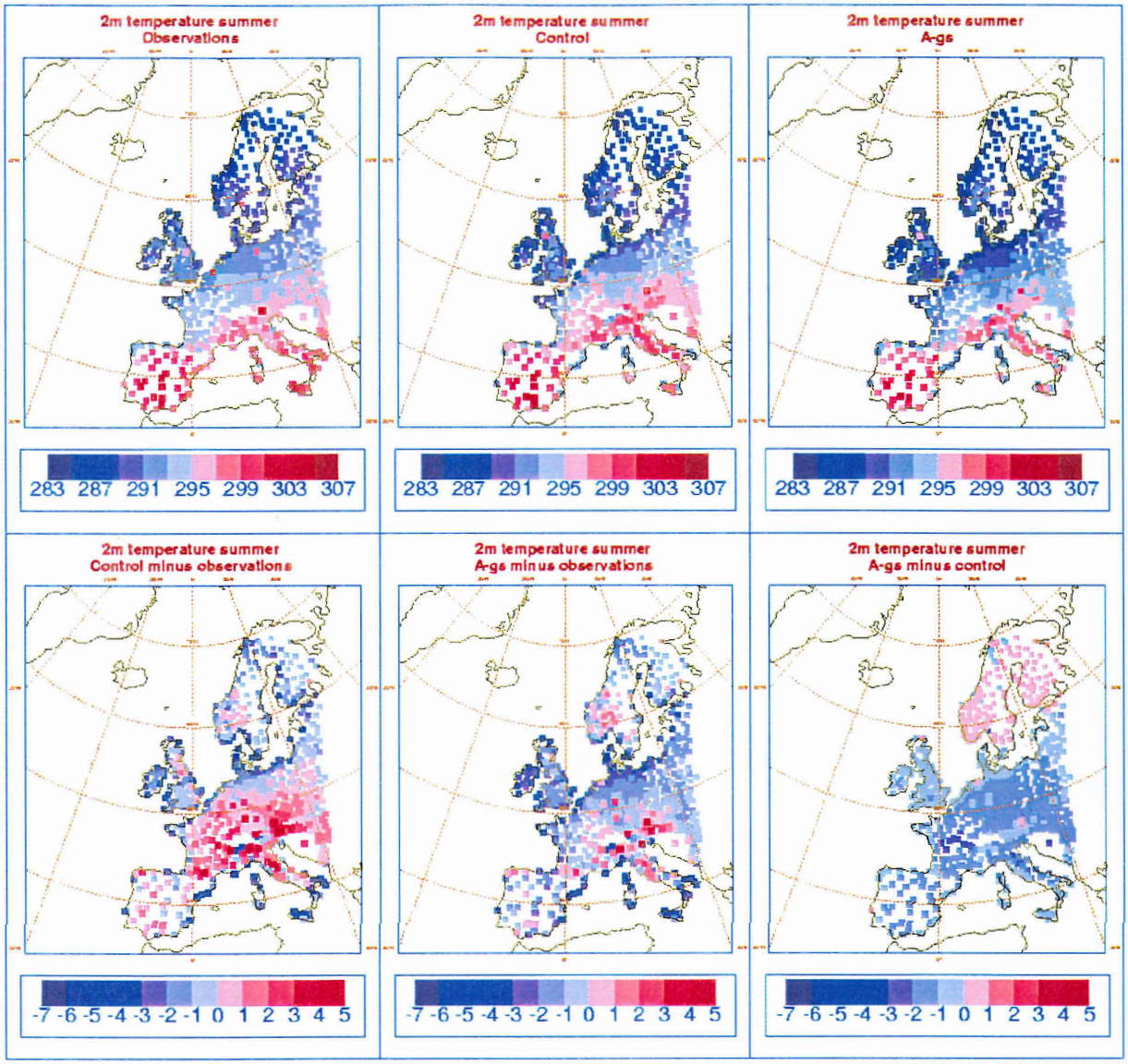

Figure 4.18. Averaged 2m temperature (K) over summer. Upper pictures: observations, control run and A-gs run. Lower pictures: differences between the control run and observations, A-gs run and observations and A-gs run and control run.

other, but on average the control run has a better correspondence with the observations than the A-gs run (smaller bias). This also can be seen in figure 4.20, where the bias and the RMS are plotted.

The A-gs model systematically overestimates the relative humidity, but the RMS has reduced, suggesting the A-gs model has a better spatial correspondence with the observations. The A-gs model predicts the large decline in June and the large increase in August more accurately than the control model. The difference in RMS error is smallest in summer and autumn.

In figure 4.21 the temperature is given. In spring both models almost perfectly agree with the observations. In summer and autumn the temperature is underestimated, while in summer the difference between the A-gs model and the observations is larger than the difference between the control model and the observations.

In figure 4.22 this effect can be seen also. The correspondence is well, but decreases in summer and autumn. The RMS of the A-gs run however has become smaller in summer and autumn, just as for the relative humidity.

From these figures it can be concluded that on average the A-gs model has a positive bias

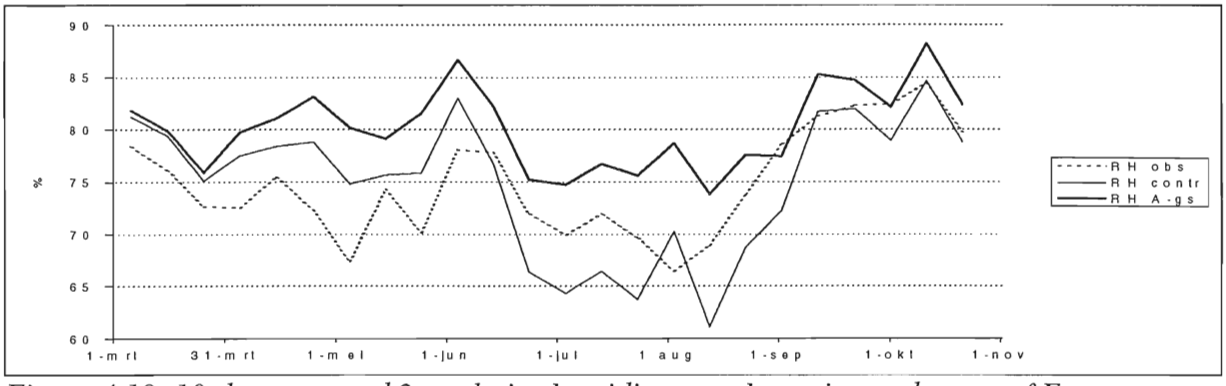

Figure 4.19. 10-day averaged 2m relative humidity over the entire study area of Europe.

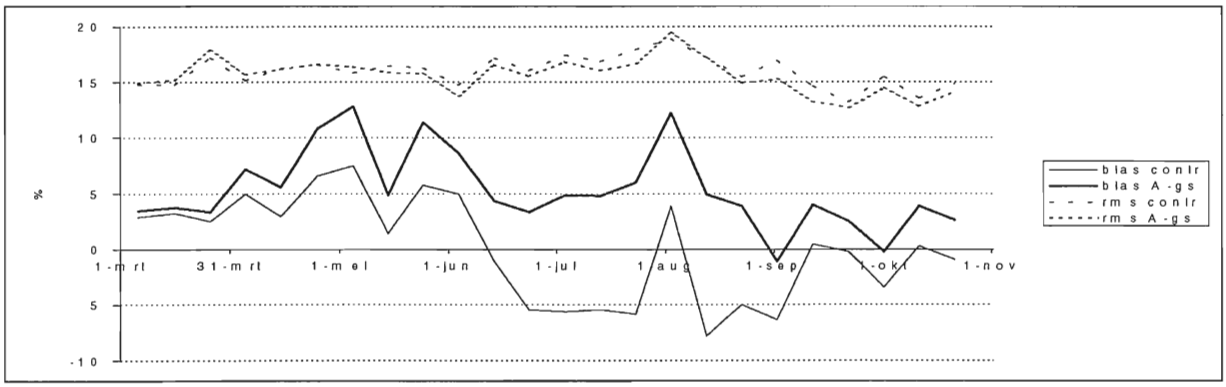

Figure 4.20. 10-day averaged bias and unbiased root mean square error of 2m relative humidity over the entire study area of Europe.

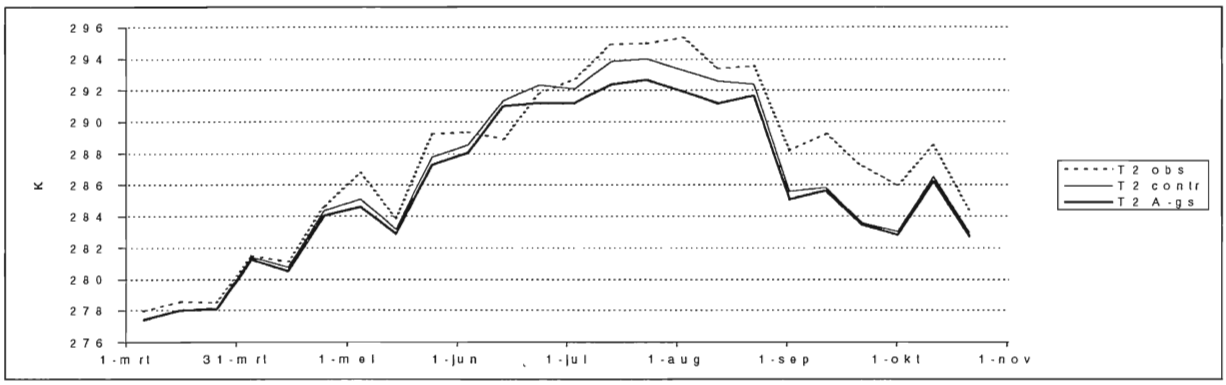

Figure 4.21. 10-day averaged 2m temperature over the entire study area of Europe.

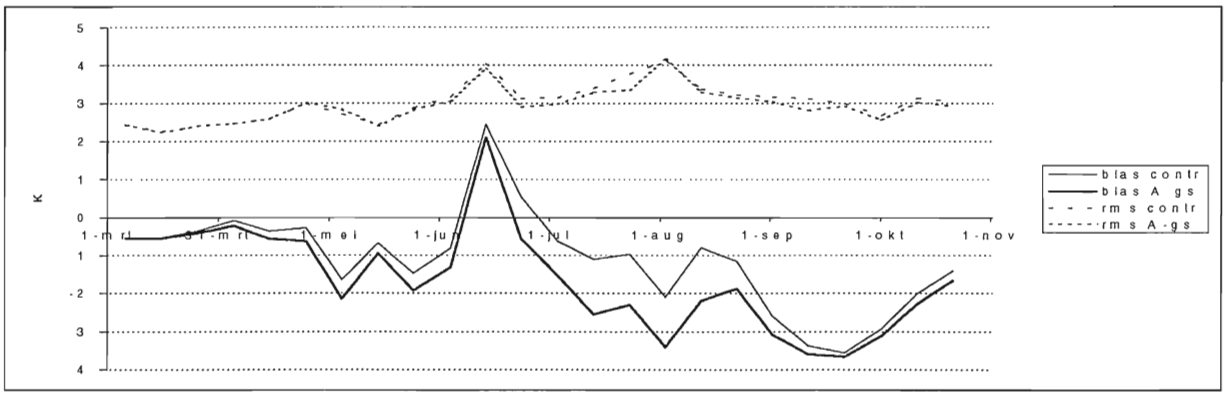

Figure 4.22. 10-day averaged bias and unbiased root mean square error of 2m air temperature for over the entire study area of Europe.

regarding the relative humidity and a negative bias regarding the temperature, but the RMS has become smaller in comparison to the control model. This phenomenon can be understood as follows: the averaged bias of the control run is small, but the variance is larger. The averaged bias of the A-gs run is larger, but the variance is smaller, i.e. the A-gs model is more able to describe the fluctuations than the control model, although a systematic error occurs. This systematic error is probably partially due to the non-equilibrium initialisation of the model, causing the A-gs model to systematically overestimate the latent heat flux and causing multiple other effects. Also the representation of high vegetation could have some influence.

4.2.2 Study area 1: low vegetation surfaces

In figure 4.23 the energy budget over low vegetation is given. As expected from the previous maps, the latent heat flux has increased and the sensible heat flux has decreased. The largest differences occur in summer. The net radiation somewhat increased (meaning a lower skin temperature) and the soil heat flux somewhat decreased. The hydrological budget for low vegetation is shown in figure 4.24. Precipitation and evaporation have increased and in summer the large decrease of soil moisture is clear.
More interesting are figures 4.25 and 4.26 showing the relative humidity. In spring the relative humidity is overestimated by both models. In June the large decrease in relative humidity is clear, but here also the decline for the A-gs run is not as big as that for the control run, so again the A-gs model has a better correspondence with the observations. Even more interesting is the large decrease of the RMS error in summer and autumn. Still the relative humidity is systematically overestimated.
In figure 4.27 the temperature is compared with observations. Here also the temperature is too low for both models, with the largest differences in summer and autumn. In figure 4.28 it can be seen that the RMS in the temperature has become smaller, so here also the A-gs model is more accurate (regarding the variance) than the control model. It appears that due to the dry summer a systematic error has been introduced in the RACMO: a too low temperature and a decreased relative humidity (see figures 4.20 and 4.26).

4.2.3 Study area 2: high vegetation surfaces

From the previous maps, showing the spatial distribution of some relevant quantities, large differences could be seen over high vegetation areas. The suspicion has risen whether high vegetation (needle-leaf trees excluded) was well represented by the A-gs model.
In figure 4.29 the energy budget is given over high vegetation. Large differences in latent and sensible heat occur between both models (larger than for low vegetation). Also the net radiation has increased more. The hydrological budget (figure 4.30) also shows some larger differences. The evaporation has increased much more than for low vegetation (notice the different scale in comparison with figure 4.24). Also less soil moisture is available in November.
In figures 4.31 and 4.32 the relative humidity is compared with observations. On average the control model has a better performance than the A-gs model. Both models predict a correct relative humidity in early spring and autumn, but in summer the relative humidity is overestimated by the A-gs model. However, the RMS is lower.
According to figure 4.33 the temperature is predicted well in spring by both models. In summer the temperature of the A-gs model is too low and in autumn both models are too low, as seen in the former figures. From figure 4.34 it can be seen that the RMS has become smaller in summer and autumn for the A-gs run.

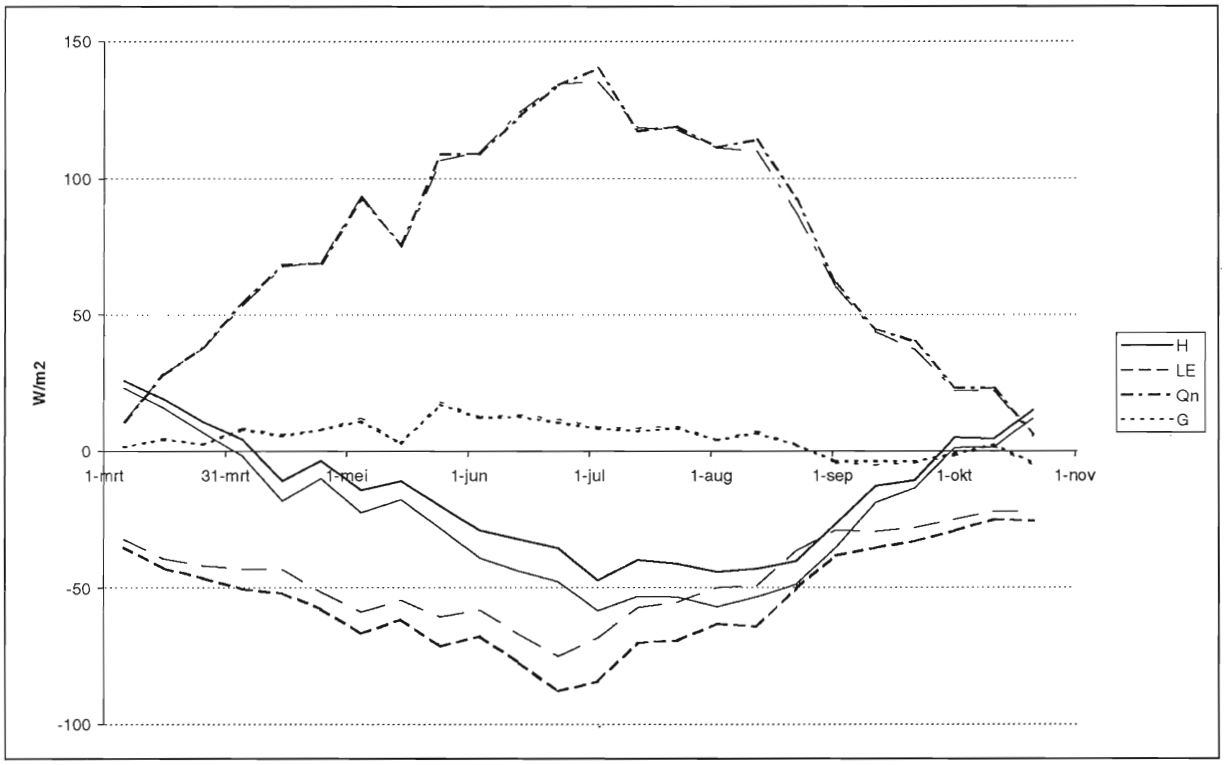

Figure 4.23. 10-day averaged sensible and latent heat flux, net radiation and soil heat flux over low vegetation surface. Thin lines: control run. Thick lines: A-gs run.

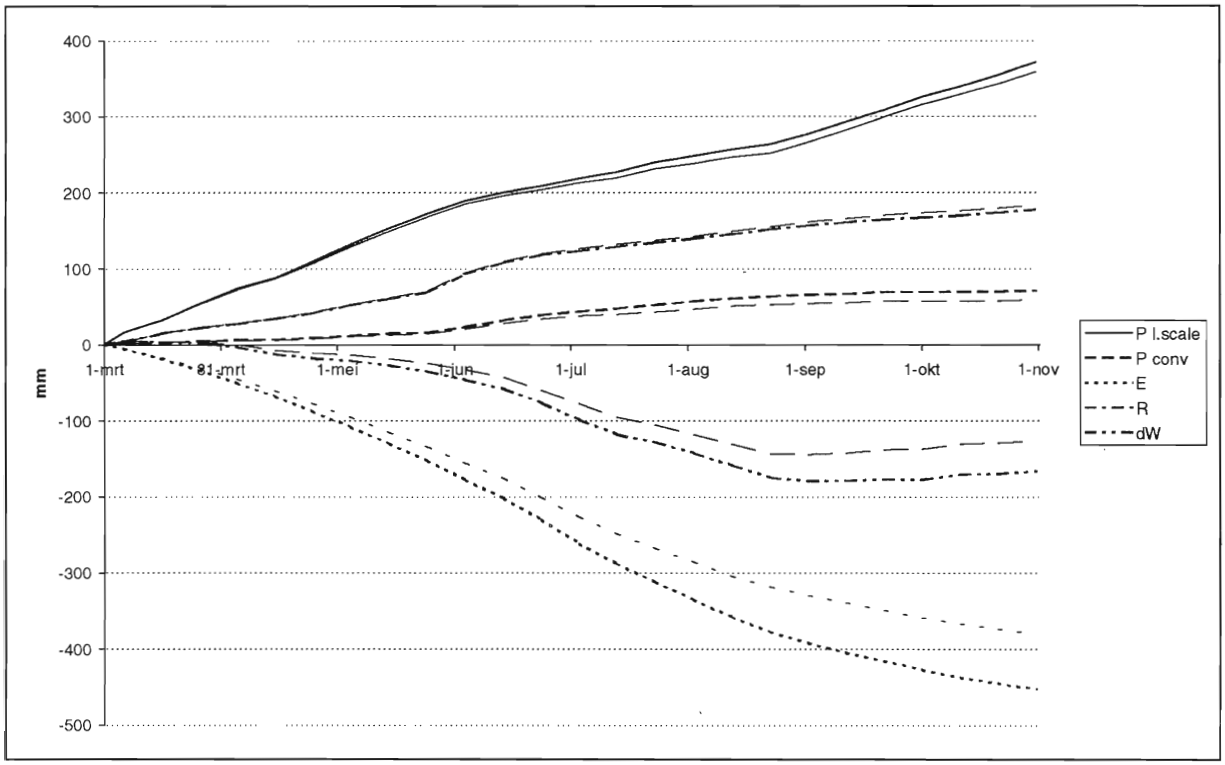

Figure 4.24. Cumulative large-scale and convective precipitation, evaporation, total runoff and change of soil water storage over low vegetation surface. Thin lines: control run. Thick lines: A-gs run.

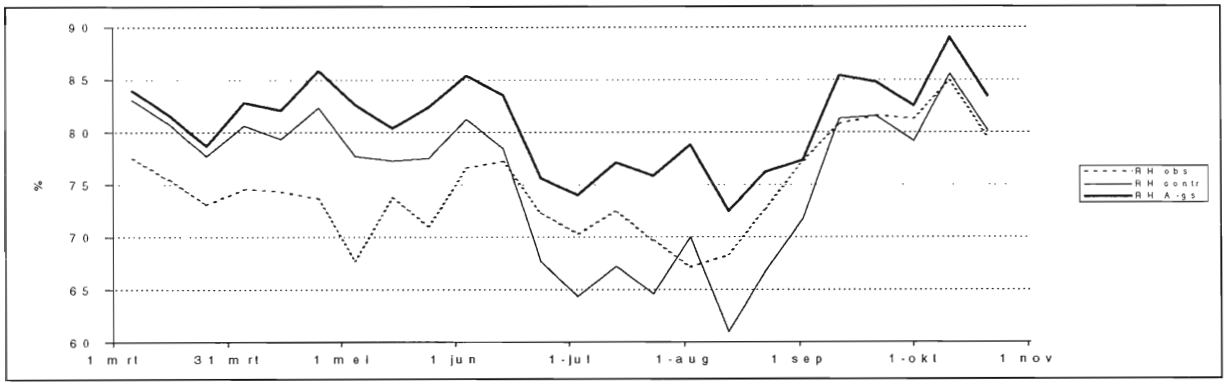

Figure 4.25. 10-day averaged 2m relative humidity over low vegetation surface.

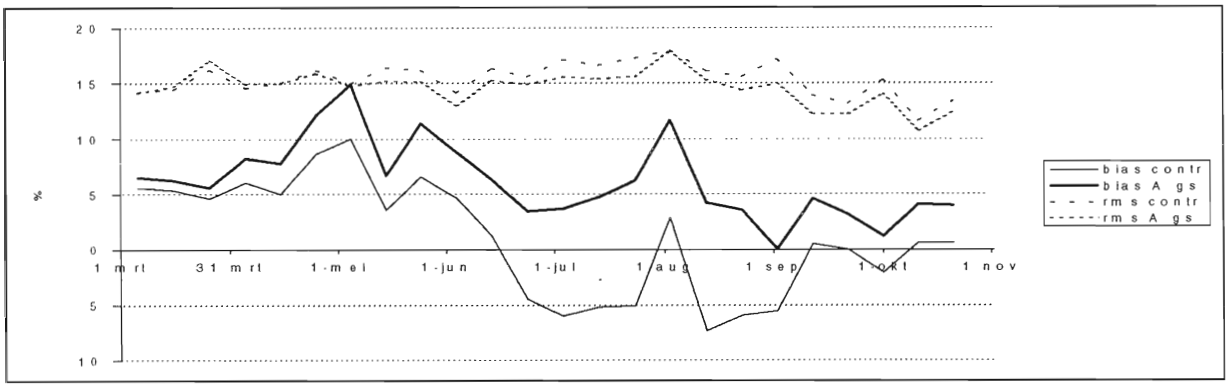

Figure 4.26. 10-day averaged bias and unbiased root mean square error of 2m relative humidity over low vegetation surface.

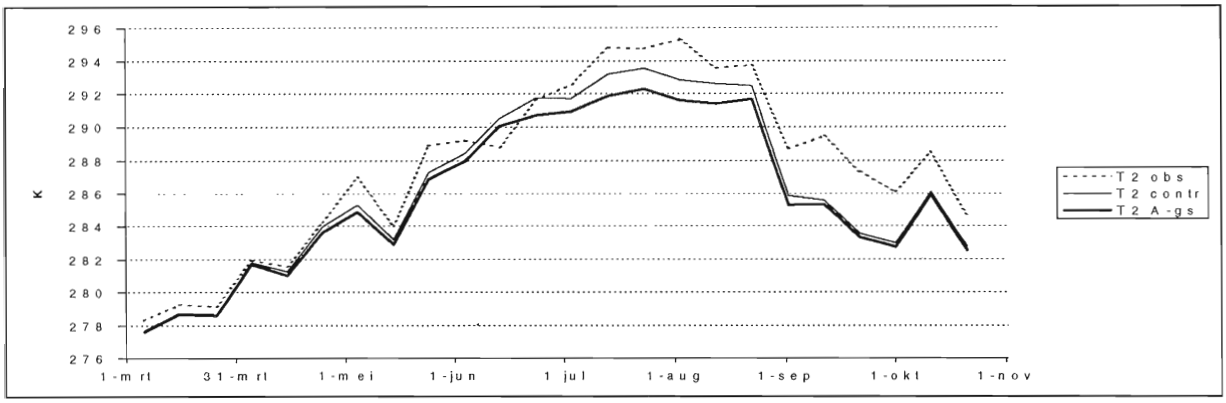

Figure 4.27. 10-day averaged 2m temperature over low vegetation surface.

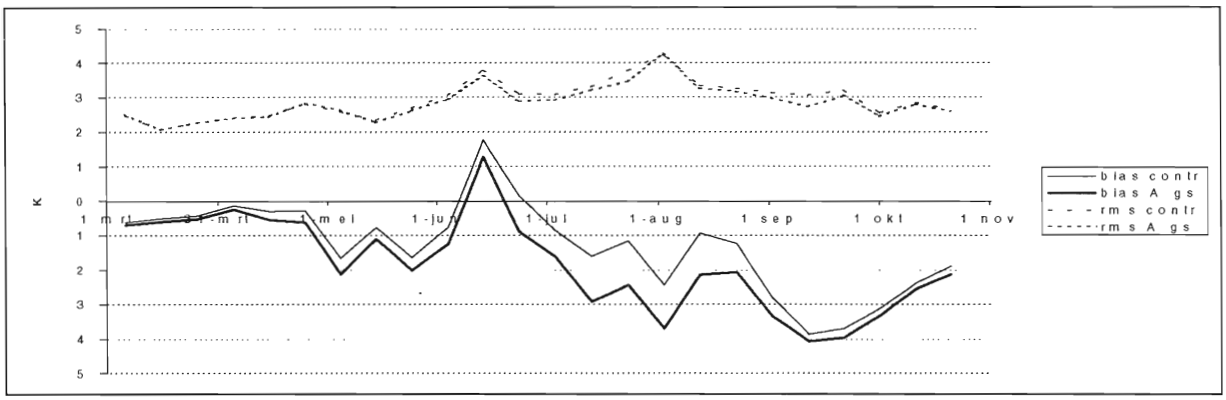

Figure 4.28. 10-day averaged bias and unbiased root mean square error of 2m air temperature over low vegetation surface.

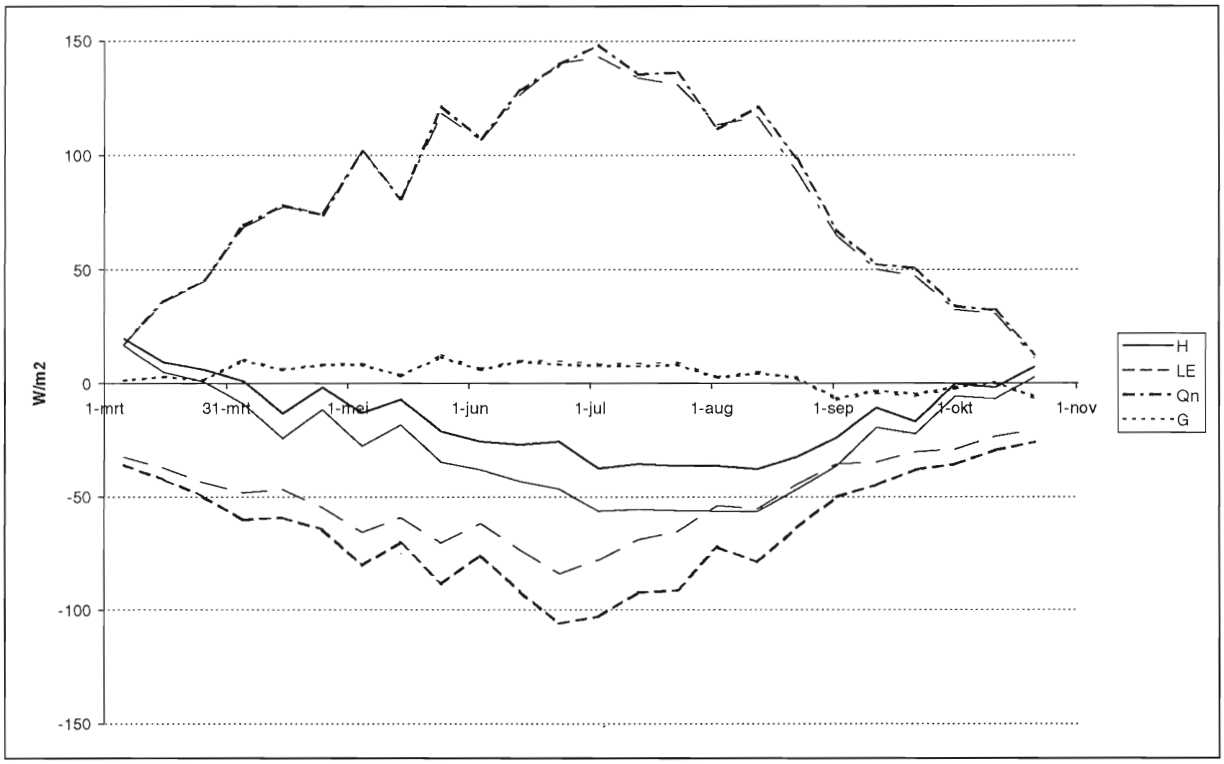

Figure 4.29. 10-day averaged sensible and latent heat flux, net radiation and soil heat flux over high vegetation surface (needle-leaf trees excl.). Thin lines: control run. Thick lines: A-gs run.

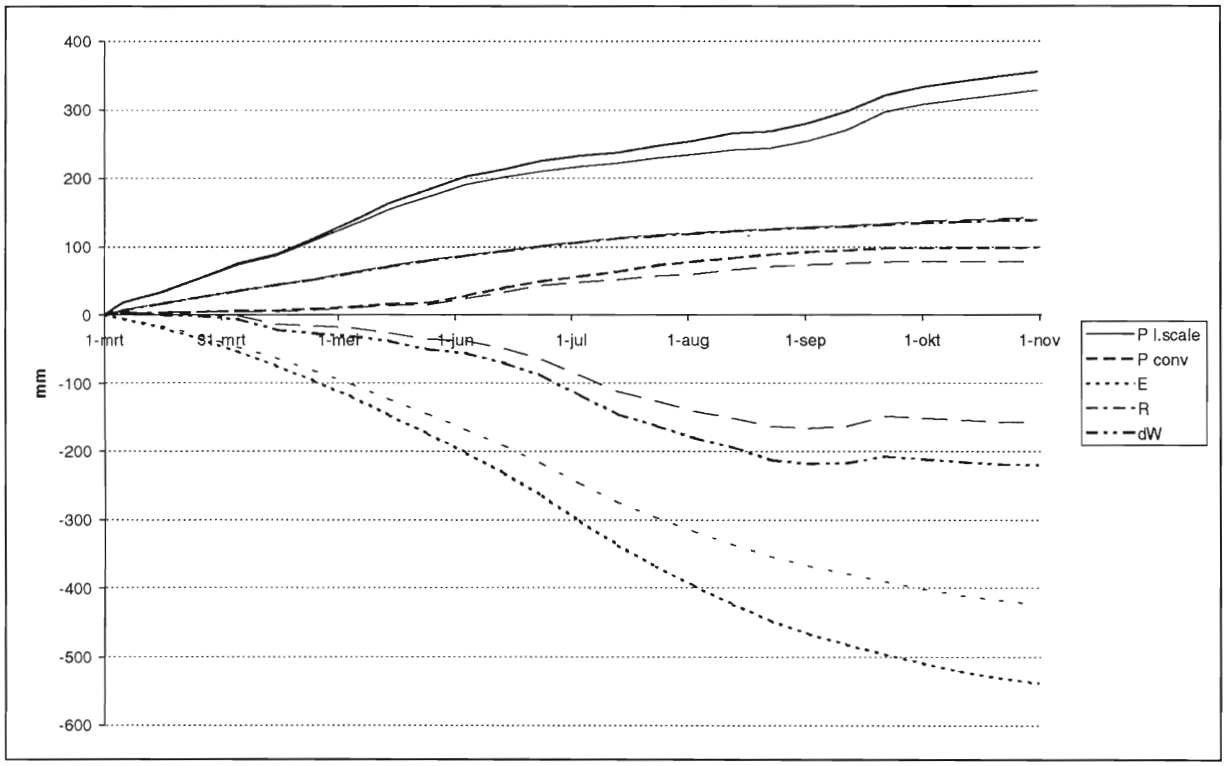

Figure 4.30. Cumulative large-scale and convective precipitation, evaporation, total runoff and change of soil water storage over high vegetation surface (needle-leaf trees excl.). Thin lines: control run. Thick lines: A-gs run.

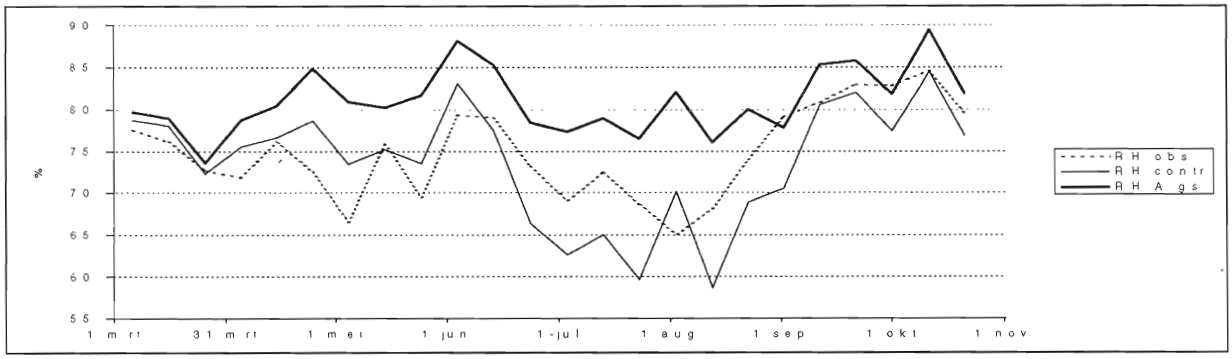

Figure 4.31. 10-day averaged 2m relative humidity over high vegetation surface (needle-leaf trees excl.).

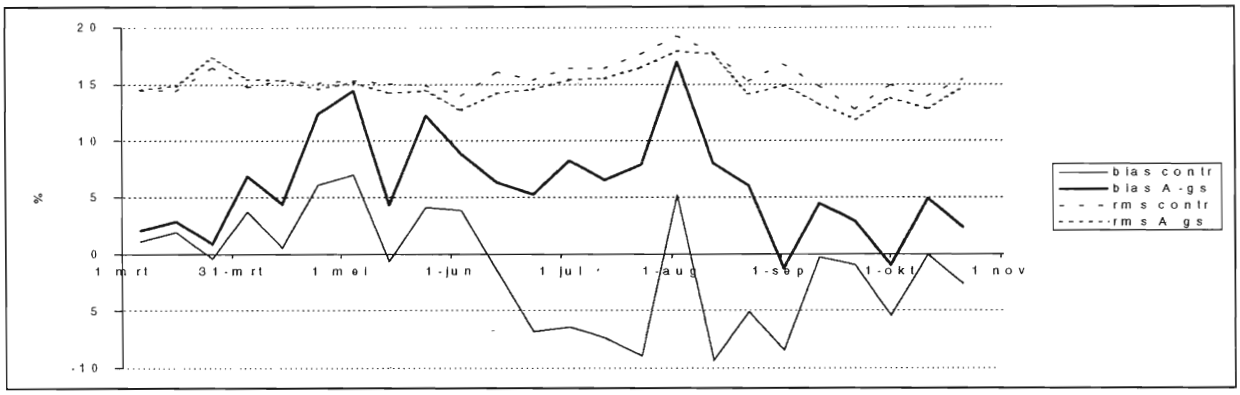

Figure 4.32. 10-day averaged bias and unbiased root mean square error of 2m relative humidity over high vegetation surface (needle-leaf trees excl.).

Figure 4.33. 10-day averaged 2m temperature over high vegetation surface (needle-leaf trees excl.).

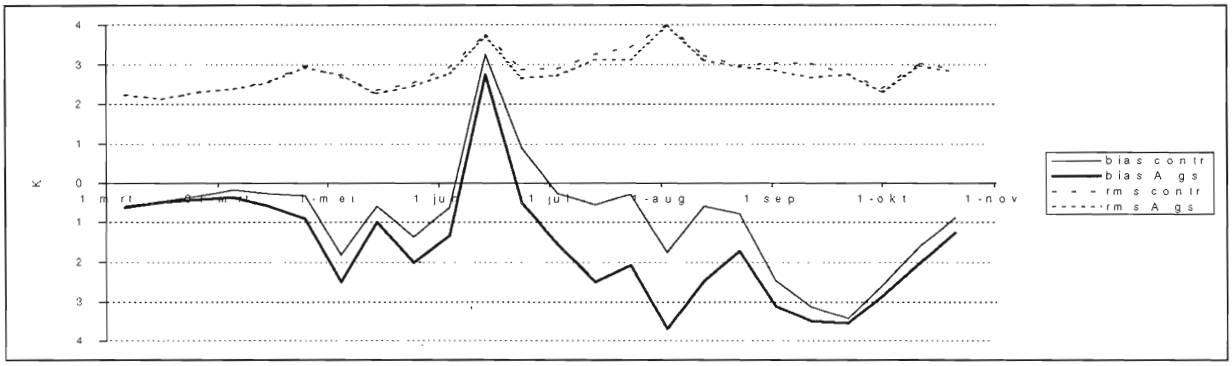

Figure 4.34. 10-day averaged bias and unbiased root mean square error of 2m air temperature over high vegetation surface (needle-leaf trees excl.).

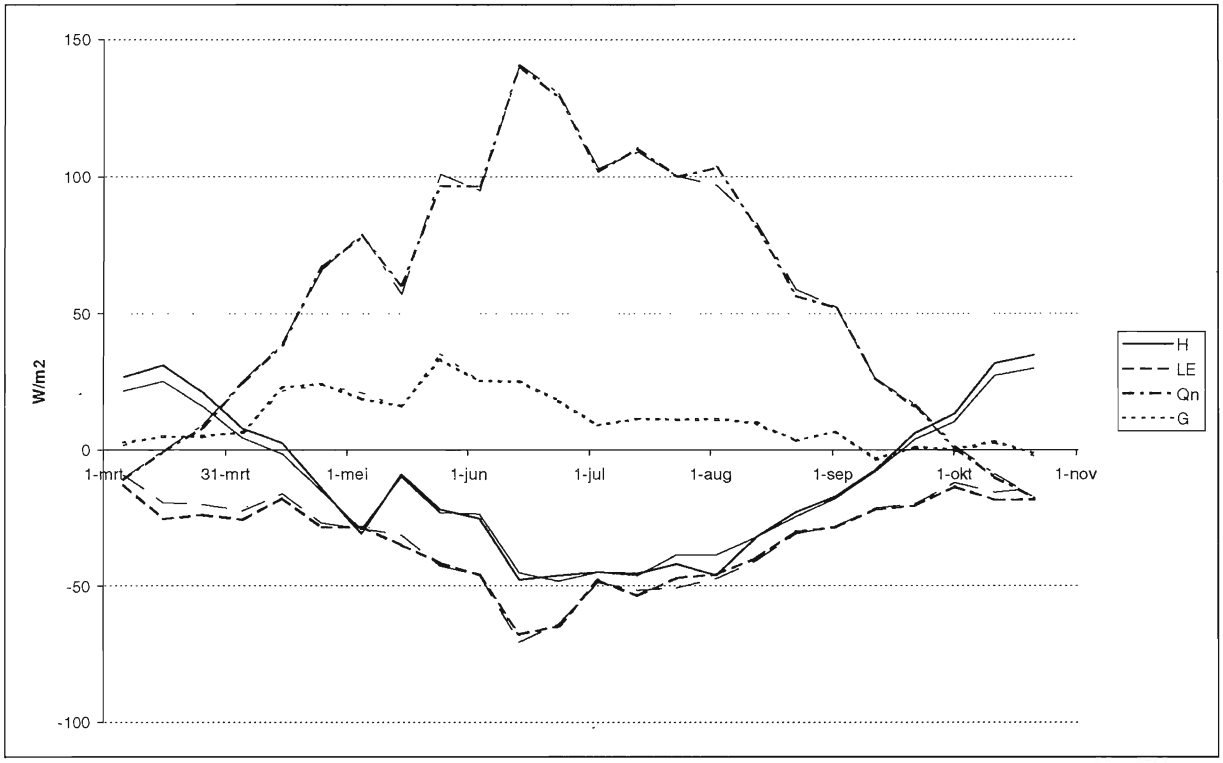

Figure 4.35. 10-day averaged sensible and latent heat flux, net radiation and soil heat flux over needle-leaf trees. Thin lines: control run. Thick lines: A-gs run.

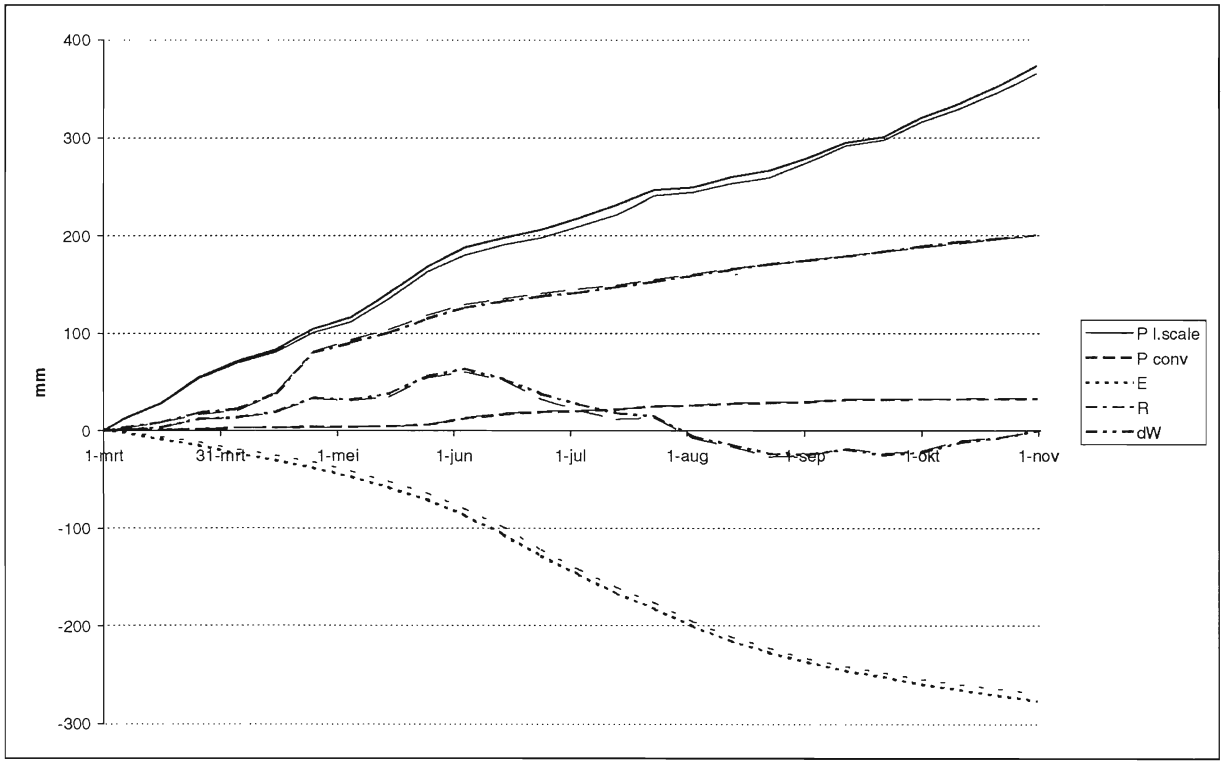

Figure 4.36. Cumulative large-scale and convective precipitation, evaporation, total runoff and change of soil water storage over needle-leaf trees. Thin lines: control run. Thick lines: A-gs run.

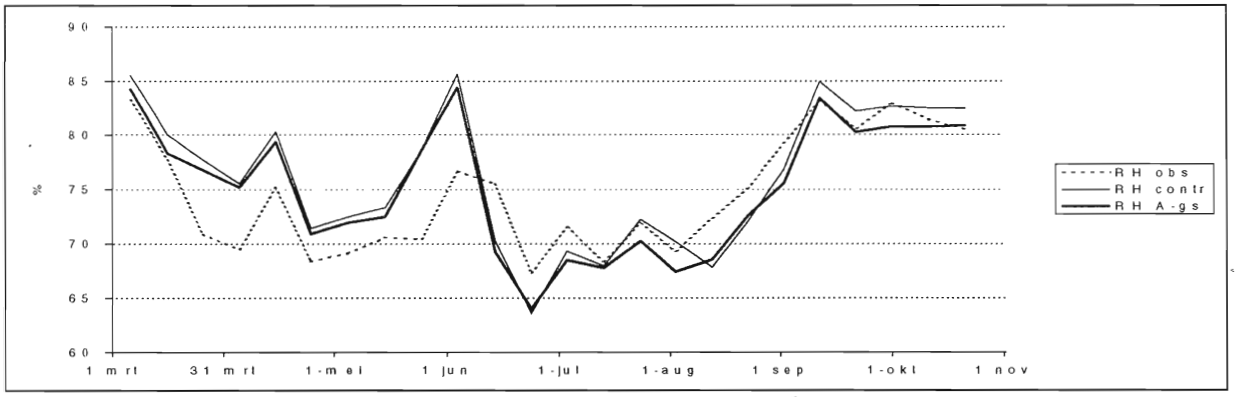

Figure 4.37. 10-day averaged 2m relative humidity over needle-leaf trees.

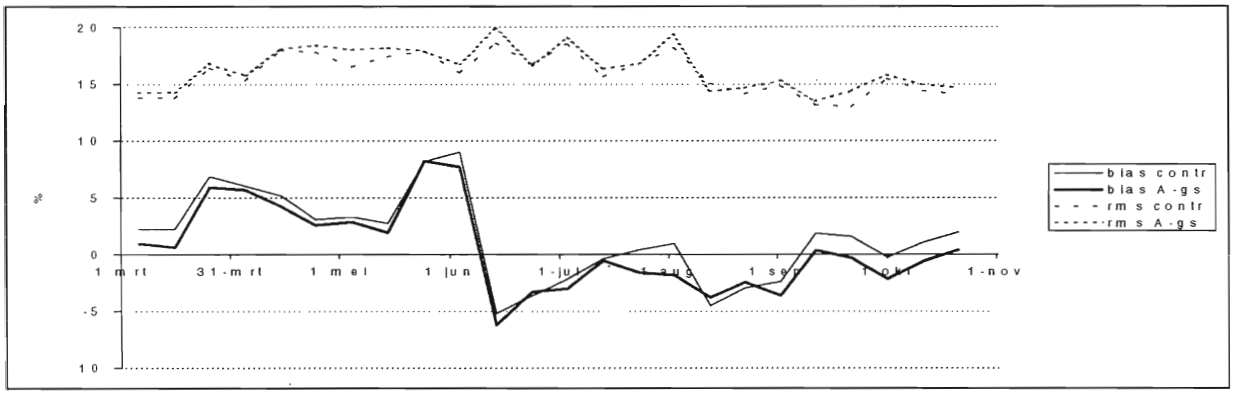

Figure 4.38. 10-day averaged bias and unbiased root mean square error of 2m relative humidity over needle-leaf trees.

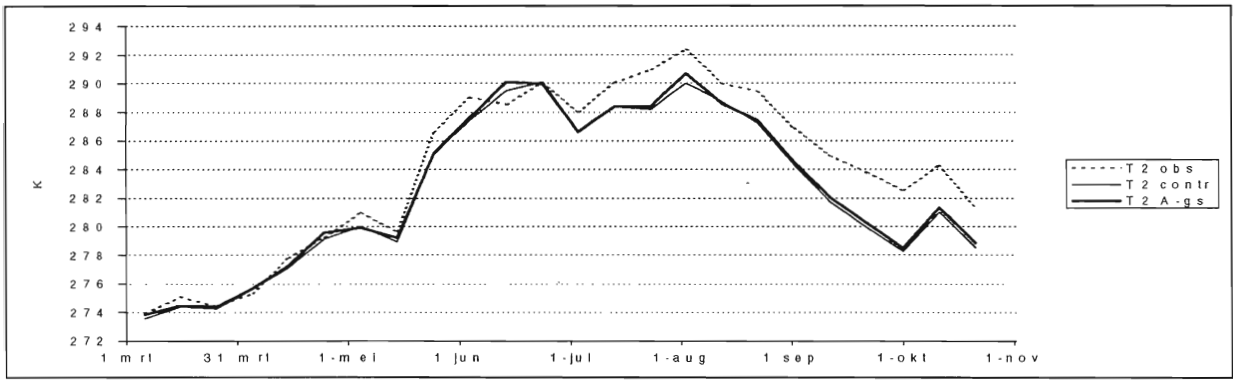

Figure 4.39. 10-day averaged 2m temperature over needle-leaf trees.

Figure 4.40. 10-day averaged bias and unbiased root mean square error of 2m air temperature over needle-leaf trees.

From these figures one may conclude that high vegetation is misrepresented by the A-gs model: the differences in the energy and hydrological budget are larger and the biases in relative humidity and temperature are larger than for low vegetation. Due to the A-gs approach the evaporation has increased over high vegetation surfaces. Also the initial soil moisture content may play a role, so the increased evaporation may not be attributed only to the A-gs model itself.

4.2.4 Study area 3: needle-leaf trees

For the needle-leaf trees the energy and hydrological budgets are shown in figures 4.35 and 4.36. As expected, the differences between both models are very small. The main reason may be the fact that the A-gs model parameters are fit to the control model.
Probably as a result of the parameter fitting for needle-leaf trees, the decline in relative humidity in June is not as well represented by the A-gs model as it did for the other vegetation types. Still the bias is small, but the RMS increased, see figures 4.37 and 4.38. Both models show a higher RMS for needle-leaf trees than for low vegetation or high vegetation, which is very typical.
From figures 4.39 and 4.40, it can be concluded that both models predict the temperature well, but here also the systematic underestimation in summer and autumn is present. The RMS of the A-gs model somewhat decreased.

4.3 Summary and conclusions

The implementation of the A-gs model in the ECMWF surface scheme has led to significant changes in the energy and water budged of the surface and soil. Most important feature of the A-gs approach is that evaporation has increased, leading to numerous effects.
Due to the increased evaporation, less energy is available for the sensible heat flux. Furthermore, the surface has cooled. This affects the radiation budget of the skin layer: a lower skin temperature leads to a decreased outgoing longwave radiation and hence, a higher net radiation. The soil heat flux has decreased because the temperature difference between the upper soil and the skin layer has become smaller. The changes in net radiation and soil heat flux are only small, but it must be remembered that a change of 1 W/m^2 in net radiation equals a change of 0.2 K in skin temperature.
2m relative humidity has increased for two reasons. First, more water vapour is present in the atmosphere (higher specific humidity) and second, the 2m temperature has decreased (lower saturated specific humidity) due to the smaller sensible heat flux.
The soil moisture content has decreased because more water is extracted from the soil. This is partly compensated by an increased precipitation, but areas with the largest changes in precipitation do not match the areas with the largest changes in soil moisture content.
On average these effects are most evident in areas with dominant high vegetation (area 2). Probably the A-gs approach is not fully suitable for that vegetation type. The increased evaporation over the low vegetation areas (and the high vegetation surfaces as well) is probably caused by the fact that the initial state of A-gs model run was not in equilibrium: the soil moisture content was too high, leading to an excessive evaporation during spring and summer.
By comparing the model output with observations, it can be concluded that for all vegetation types the 2m relative humidity is overestimated by both models in spring. In summer it is only overestimated by the A-gs model, while it is underestimated by the control model. In autumn both models perform well. The 2m temperature is predicted correctly by both models in spring. In summer both models underestimate the 2m temperature, where it is underestimated

more by the A-gs model. In autumn both models agree with each other, but they both underestimate the observed 2m temperature.
The performance of the A-gs model is better for low vegetation than for high vegetation. The RMS error in for 2m relative humidity and temperature has decreased by the A-gs model, but the bias has increased, probably partially due to the model initialisation. No or small improvements are achieved for needle-leaf trees. Regarding the results from chapter 3 about the offline validation and the results from this chapter about the 3D validation, it may be concluded that the A-gs model by Ronda et al. (2001) can be an improvement in modelling the surface energy budget in atmospheric models.

5. Recommendations for further research

From the results of the previous chapters it was seen the latent heat flux was overestimated by the A-gs model. A probable reason was the initial state of the A-gs run, in which soil moisture was too high. By reducing soil moisture less water is available for evaporation and as a consequence the excessive evaporation should be reduced. The modelled 2m relative humidity should then decrease and the 2m temperature should increase, both reducing the high biases. In combination with the lower RMS error, the A-gs model should have better performance than the control model in an equilibrium condition.

A model error that has little to do with the A-gs model are the surface classification and vegetation types based on the USGS NOAA global dataset (USGS, 1999). As seen in chapter 4, almost the entire European continent is covered with so called interrupted forest. Another database, for example the PELCOM land cover database, should be used the make a new surface classification. The PELCOM database does have less vegetation types (for example, there is no distinction between evergreen and deciduous vegetation), but can certainly be more accurate concerning the low vegetation/high vegetation distribution across Europe.

Mentioned earlier in chapter 4, a misrepresentation of high vegetation in the A-gs model could be present. The A-gs model should therefore be validated with a proper dataset of a broadleaf forest. The assumption that the plant physiological parameters of the A-gs model are the same for low vegetation as for broadleaf trees should be addressed in further research, focussing on e.g. the light distribution and extinction in forests.

Needle-leaf forests are certainly a subject of further investigation. As seen from the results, optimising the parameters of the A-gs model makes the model suitable for needle-leaf trees, but it does not lead to a lower bias or RMS error. It is assumed that the needles are covered with a wax layer that reduces the exchange of water vapour and CO_2. A study could be done to investigate the physiological impact of the wax layer.

Using the A-gs model, one could obtain accurate CO_2 fluxes. In this study this was not done, but it certainly can be subject of further research. As an example, model output can be compared with observations of CO_2 fluxes. Furthermore, the A-gs model could be implemented in a climate model, where increased CO_2 fluxes can be taken into account in the surface parameterisation.

References

Beljaars, A.C.M. and F.C. Bosveld, 1997: Cabauw data for the validation of land surface parameterisation schemes; J. Climate 10, 1172-1193.

Beljaars, A.C.M. and A.A.M. Holtslag, 1991: Flux parameterisation over land surfaces for atmospheric models; J. Appl. Meteor. 30, 327-341.

Beljaars, A.C.M. and P. Viterbo, 1994: The sensitivity of winter evaporation to the formulation of aerodynamic resistance in the ECMWF model; Bound. Layer Meteor. 71, 135-149.

Betts, A.K. and J.H. Ball, 1998: FIFE surface climate and site averaged dataset 1987-89; J. Atmos. Sci. 55, 1091-1108.

Betts, A.K., P. Viterbo, A.C.M. Beljaars, H.L. Pan, S.Y. Hong, M. Goulden and S. Wofsy, 1998: Evaluation of land surface interaction in ECMWF and NCEP/NCAR reanalysis models over grassland (FIFE) and boreal forest (BOREAS); J. Geophys. Res. 103, 23079-23085.

Bosveld, F.C., 1997: Derivation of fluxes from profiles over a moderately homogeneous forest; Bound. Layer. Meteor. 84, 289-327.

Chen, T.H. and co-authors, 1997: Cabauw experimental results from the project for intercomparison of land surface parameterisation schemes; J. Clim. 10, 1194-1215.

Christensen J.H., et al., 1996: The HIRLAM4 Regional Atmospheric Climate Model. Danisch Meteorl. Institute, Copenhagen. Scientific Report 96-4, 51 pp.

Dickinson R.E., A. Henderson-Sellers, P.J. Kennedy (1993): Biosphere-Atmosphere Transfer Scheme (BATS) for the NCAR Community Climate model; NCAR Technical Note NCAR/TN-275+STR, 72 pp.

Douville, H.J., F. Royer and J.F. Mahfouf, 1995: A new snow parameterisation for the Meteo France climate model. Part I: validation in stand alone experiments; Clim. Dynamics 12. 21-35.

Ek, M. and A.A.M. Holtslag, 1999: Interaction of the atmospheric boundary layer with the land surface: a case study at Cabauw; Proceedings AMS Symposium on boundary layers and turbulence.

Goulden, M.L., B.G. Daube, S.M. Fan, D.J. Sutton, A. Bazzaz. J.W. Munger and S.C. Wofsy, 1998: Physiological responses of a black spruce forest to weather; J. Geophys. Res. D102, 28987-28996.

Gustafsson, N., 1993: HIRLAM 2 final report; available from SMHI, S60-176, Norrköpping, Sweden.

Van den Hurk, B.J.J.M., P. Viterbo, A.C.M. Beljaars and A.K. Betts, 2000: Offline validation of the ERA40 surface scheme; ECMWF Technical Memorandum; ECMWF-TM 295, 42 pp.

Jacobs, C.M.J., 1994: Direct impact of atmospheric CO_2 enrichment on regional transpiration; Ph.D. thesis Wageningen Agricultural University, Wageningen.

Jarvis, P.G., 1976: The interpretation of the variations in leaf water potential and stomatal conductance found in canopies in the field; Phil. Trans. R. Soc. Lond. Ser. B, 273, 593-610.

Lövenstein, H., E.A. Lantinga, R. Rabbinge and H. van Keulen, 1995: Course book principles of production ecology; Department of Theoretical Production Ecology, Wageningen University.

Roeckner, E., et al., 1996: The atmospheric general circulation model ECHAM4: Model description and simulation of present-day climate; Max Planck Institute für Meterologie, Report No. 218.

Ronda, R.J., H.A.R. de Bruin and A.A.M. Holtslag, 2001: Representation of the canopy conductance in modelling the surface energy budget for low vegetation; (in preparation).

Sellers, P.J. and co-authors, 1998: BOREAS in 1997: Experiment overview, scientific results and future directions; J. Geophys. Res. D102, 28731-28769.

Shewchuk, S., 1998: Surface mesonet for BOREAS; J. Geophys. Res. D102, 29077-29082.

Shuttleworth, W.J. and co-authors, 1984: Eddy correlation measurements of energy partition for Amazonian forest; Q. J. Roy. Meteor. Soc. 110, 1143-1162.

Shuttleworth, W.J., 1988: Evaporation from Amazonian rainforest; Proc. R. Soc. Lond. 233, 321-346.

Stewart, J.B., 1988: Modelling surface conductance of pine forest; Agric. For. Meteor., 30, 111-127.

USGS, 1999: see http://edcwww.cr.usgs.gov/landdaac/glcc/glcc.html.

IJpelaar, R.J.M., 2000: Evaluation of modified soil parameterisation in the ECMWF land surface scheme; KNMI TR-228.

Zhang, H. and P.S. Nobel, 1996: Dependency of Ci/Ca and leaf transpiration efficiency on the vapour pressure deficit; Aust. J. Plant Physiol., 232, 561-568.

Appendices

Appendix I Implementation of the A-gs model in the RACMO

In the A-gs model the canopy resistance is calculated using a semi-empirical plant physiological model. The A-gs model is to be implemented in the RACMO surface scheme, replacing the empirical-statistical model. In this appendix a summary will be given about the changes made to the RACMO by implementation the A-gs model
In the RACMO the canopy resistance PWET is calculated in the subroutine VDFSURF. In the old model a minimal canopy resistance is used in combination with three stress functions: a soil moisture stress function, a radiation stress function and an atmospheric moisture deficit stress function. In VDFSURF the minimal canopy resistance, the radiation stress function and the atmospheric moisture deficit stress function are replaced with A-gs approach.
The A-gs model parameters are based on a distinction in C3, C4 and needle-leaf plants. Therefore a new variable in VDFSURF is introduced, KCPL (KCPLL or KCPLH for low or high vegetation). This variable is indicating whether the vegetation type consists of C3 plants, C4 plants or needle-leaf trees. The labelling of the vegetation types is done in the subroutine SUVEG by introducing a new variable KVCPL. This variable is set to 1 for C3 plants, 2 for C4 plants and 3 for needle-leaf trees. In the subroutine YOEVEG the variable KVCPL is declared. Two new subroutines are made. In subroutine SUAGS the A-gs model parameters are given values. In subroutine YOEAGS the A-gs model parameters are declared. SUAGS is called in SUPHEC. In VDFSURF a new function FCEXPINT is called. This function calculates an exponential integral needed in the A-gs model.
Also a new variable is PQSAM1, the apparent surface humidity at T-1. This variable is needed to compute the surface moisture deficit. The parameters RVRSMIN (ZRSMIN in VDFSURF) and RVHSTR (ZHSTR in VDFSURF) are removed from SUVEG and YOEVEG, because they are not used anymore in VDFSURF. Below a summary is given of the changes made to the RACMO.

Changes made to subroutine VDFSURF (prepares surface boundary condition for T and Q):

- New module called:
  YOEAGS (declaration of the model parameters)

- New function called:
  FCEXPINT (E1) (computes the exponential integral)

- New code:
  A-gs model

- New variables:
  KCPL (C3/C4/needleleaf plant type label)
  PSRFL (net short wave radiation, needed for PAR)
  PQSAM1 (surface humidity at T-1)

Changes made to subroutine SUVEG (setup vegetation parameters):

- New code:
  C3/C4/needleleaf plant type label for each vegetation type

- New variables:
  KVCPL (C3/C4/needleleaf plant type label)

Changes made to module YOEVEG (declaration vegetation parameters):

- New variable:
  KVCPL (C3/C4/needleleaf plant type label)

Changes made to subroutine VDFMAIN (vertical exchange by turbulence):

- Calling VDFSURF, ZSRFD (incoming short wave radiation) is replaced by PSSRFLTI (net short wave radiation for each tile)

- New variable:
  ZQSATI1 (surface humidity at T-1)

New subroutine SUAGS (setup A-gs model parameters):

- New variables:
  NCATYPES (number of plant types)
  RGAMMA25 (CO2 compensation point at 25 C)
  RGAMMAQ10 (Q10 parameter RGAMMA)
  RG25 (mesophyll conductance at 25 C)
  RGMQ10 (Q10 parameter RGM)
  RGMT1 (temperature stress parameter RGM)
  RGMT2 (temperature stress parameter RGM)
  RAMAX25 (max. primary production at 25 C)
  RAMAXQ10 (Q10 parameter RGM)
  RAMAXT1 (temperature stress parameter RAMAX)
  RAMAXT2 (temperature stress parameter RAMAX)
  RGC (min. cuticular conductance)
  RF0 (max. internal CO2/external CO2 concentration)
  RRICO (empirical constant humidity stress)
  RCS (external CO2 concentration)
  REPSILON0 (initial light use efficiency)
  REXPAR (vegetation extinction coefficient)

New module YOEAGS (declaration A-gs model parameters):

- New variables:
  NCATYPES, RGAMMA25, RGAMMAQ10, RG25, RGMQ10, RGMT1, RGMT2, RAMAX25, RAMAXQ10, RAMAXT1, RAMAXT2, RGC, RF0, RRICO, REPSILON0, RCS, REXPAR

Changes made to subroutine SUPHEC (setup initialisation constants in parameterisation):

- Call SUAGS (setup A-gs model parameters)

Appendix II Statistical analysis

Let x be the difference between a modelled and an observed value:

$$x = x_{\mathrm{mod}} - x_{obs}$$

In statistics, x is called a variate and has random value. For comparison of the different models, the bias and the (unbiased) RMS (Root Mean Square) error are calculated. The bias is the mean of the variate x and it indicates the systematic difference between the model and the observations.

$$bias = \frac{1}{n}\sum_{i=1}^{n} x_i$$

The RMS, sometimes called the quadratic mean, is the square root of the mean squared value of the variate x. The unbiased RMS is calculated as the RMS where the influence of the bias in the variability has been eliminated. It indicates how good the model 'follows' the observations.

$$unbiased\,RMS = \sqrt{\frac{1}{n}\sum_{i=1}^{n} x_i^2 - bias^2}$$

Another way to indicate the systematic error of a model is the so-called mean error. This is the averaged relative deviation of the model output to the observations. A model with a bias equal to zero will have a mean error of 1. A systematic overestimation by the model will mean a mean error larger than 1. A systematic underestimation will mean a mean error smaller than 1. Using the least squares method, where the regression line is forced through the origin, the mean error is calculated by

$$mean\ error = \frac{\sum_{i=1}^{n} x_{obs,i} x_{\mathrm{mod},i}}{\sum_{i=1}^{n} x_{obs,i}^2}$$

Finally there is the R squared value R^2. This quantity indicates the variance in the model output explained by the variance in the observations. It is calculated by

$$R^2 = \frac{\left[n\sum_{i=1}^{n} x_{obs,i} x_{\mathrm{mod},i}\right]^2}{\left[n\sum_{i=1}^{n} x_{obs,i}^2 - \left(\sum_{i=1}^{n} x_{obs,i}\right)^2\right]\left[n\sum_{i=1}^{n} x_{\mathrm{mod},i}^2 - \left(\sum_{i=1}^{n} x_{\mathrm{mod},i}\right)^2\right]}$$

Its value is 1 for a perfect agreement with the observations and goes down to zero for no agreement at all.

OVERZICHT VAN KNMI-PUBLICATIES, VERSCHENEN SEDERT 1999

KNMI-PUBLICATIE MET NUMMER

186-II Rainfall generator for the Rhine Basin: multi-site generation of weather variables by nearest-neighbour resampling / T. Brandsma a.o.

186-III Rainfall generator for the Rhine Basin: nearest-neighbour resampling of daily circulation indices and conditional generation of weather variables / Jules J. Beersma and T. Adri Buishand

186-IV Rainfall generator for the Rhine Basin: multi-site generation of weather variables for the entire drainage area / Rafal Wójcik, Jules J. Beersma and T. Adri Buishand

188 SODA workshop on chemical data assimilation: proceedings; 9-10 December 1998, KNMI, De Bilt, The Netherlands

189 Aardbevingen in Noord-Nederland in 1998: met overzichten over de periode 1986-1998 / [Afdeling SO]

190 Seismisch netwerk Noord-Nederland / [afdeling Seismologie]

191 Het KNMI-programma HISKLIM (HIStorisch KLIMaat) / T. Brandsma, F. Koek, H. Wallbrink, G. Können

192 Gang van zaken 1940-48 rond de 20.000 zoekgeraakte scheepsjournalen / Hendrik Wallbrink en Frits Koek

193 Science requirements document for OMI-EOS / contr. by R. van der A .. [et al.] **(limited distribution)**

194-1 De zonsverduistering van 11 augustus 1999, deel 1: de waarnemingen van het gedrag van flora en fauna / J. Kuiper, m.m.v. Guus Kauffeld

195 An optimal infrasound array at Apatity (Russian Federation) / Läslo Evers and Hein Haak **(limited distribution)**

TECHNISCH RAPPORT = TECHNICAL REPORT (TR)

216 Evaluatierapport Automatisering Visuele Waarnemingen : Ontwikkeling Meestsystemen / Wiel Wauben e.a.

217 Verificatie TAF en TREND / Hans van Bruggen

218 LEO - LSG and ECBILT coupled through OASIS: description and manual / A. Sterl

219 De invloed van de grondwaterstand, wind, temperatuur en dauwpunt op de vorming van stralingsmist: een kwantitatieve benadering / Jan Terpstra

220 Back-up modellering van windmeetmasten op luchthavens / Ilja Smits

221 PV-mixing around the tropopause in an extratropical cyclone / M. Sigmond

222 NPK-TIG oefendag 16 december 1998 / G.T. Geertsema, H. van Dorp e.a.

223 Golfhoogteverwachtingen voor de Zuidelijke Noordzee: een korte vergelijking van het ECMWF-golfmodel (EPS en operationeel), de nautische gidsverwachting, Nedwam en meteoroloog / D.H.P. Vogelezang, C.J. Kok

224 HDFg library and some hdf utilities: an extention to the NCSA HDF library user's manual &reference guide / Han The

225 The Deelen Infrasound Array: on the detection and identification of infrasound / L.G. Evers and H.W. Haak

226 2D Variational Ambiguity Removal / J.C.W. de Vries and A.C.M. Stoffelen

227 Seismo-akoestische analyse van de explosies bij *S.E. Fireworks* ; Enschede 13 mei 2000 / L.G. Evers e.a.

228 Evaluation of modified soil parameterization in the ECMWF landsurface scheme / R.J.M. IJpelaar

229 Evaluation of humidity and temperature measurements of Vaisala's HMP243 plus PT100 with two reference psychrometers / E.M.J. Meijer

230 KNMI contribution to the European project WRINCLE: downscaling relationships for precipitation for several European sites / B.-R. Beckmann and T.A. Buishand

231 The Conveyor Belt in the OCCAM model: tracing water masses by a Lagrangian methodology / Trémeur Balbous and Sybren Drijfhout

232 Analysis of the Rijkoort-Weibull model / Ilja Smits

233 Vectorization of the ECBilt model / X. Wang and R.J. Haarsma

234 Evaluation of a plant physiological canopy conductance model in the ECMWF land surface scheme / J. van de Kassteele

WETENSCHAPPELIJK RAPPORT = SCIENTIFIC REPORT (WR)

99-01 Enhancement of solar and ultraviolet surface irradiance under partial cloudy conditions / Serdal Tunç

99-02 Turbulent air flow over sea waves: simplified model for applications / V.N. Kudryavtsev et al.

99-03 The KNMI Garderen experiment, micro-meteorological observations 1988-89: corrections / Fred C. Bosveld

99-04 ASGAMAGE: the ASGASEX MAGE experiment : final report / ed. W.A.Oost

00-01 A model of wind transformation over water-land surfaces / V.N. Kudryavtsev et al.

00-02 On the air-sea coupling in the WAM wave model / D.F.Doortmont and V.K. Makin.

00-03 Salmon's Hamiltonian approach to balanced flow applied to a one-layer isentropic model of the atmosphere / W.T.M. Verkley

00-04 On the behaviour of a few popular verification scores in yes-no forecasting / C.J. Kok

01-01 Hail detection using single-polarization radar / Iwan Holleman

01-02 Comparison of modeled ozone distributions with ozonesonde observations in the tropics / Rob Put

01-03 Impact assessment of a doppler wind lidar in space on atmospheric analyses and numerical weather prediction / G.J. Marseille, A. Stoffelen, F. Bouttier, C. Cardinali, S. de Haan and D. Vasiljevic.

KNMI-bibliotheek, postbus 201, 3730 AE De Bilt, tel. 030 - 2 206 855, fax 030 - 2 210 407; bibliotheek@knmi.nl